

# The State of the Art of Hybrid RANS/LES Modeling for the Simulation of Turbulent Flows

Bruno Chaouat<sup>1</sup>

Received: 22 April 2017 / Accepted: 13 June 2017 / Published online: 1 July 2017  
© Springer Science+Business Media B.V. 2017

**Abstract** This review presents the state of the art of hybrid RANS/LES modeling for the simulation of turbulent flows. After recalling the modeling used in RANS and LES methodologies, we propose in a first step a theoretical formalism developed in the spectral space that allows to unify the RANS and LES methods from a physical standpoint. In a second step, we discuss the principle of the hybrid RANS/LES methods capable of representing a RANS-type behavior in the vicinity of a solid boundary and an LES-type behavior far away from the wall boundary. Then, we analyze the principal hybrid RANS/LES methods usually used to perform numerical simulation of turbulent flows encountered in engineering applications. In particular, we investigate the very large eddy simulation (VLES), the detached eddy simulation (DES), the partially integrated transport modeling (PITM) method, the partially averaged Navier-Stokes (PANS) method, and the scale adaptive simulation (SAS) from a physical point of view. Finally, we establish the connection between these methods and more precisely, the link between PITM and PANS as well as DES and PITM showing that these methods that have been built by different ways, practical or theoretical manners have common points of comparison. It is the opinion of the author to consider that the most appropriate method for a particular application will depend on the expectations of the engineer and the computational resources the user is prepared to expend on the problem.

**Keywords** Turbulence modeling · RANS modeling · LES simulation · Hybrid RANS-LES methods · VLES · DES · PITM · PANS · SAS

---

✉ Bruno Chaouat  
Bruno.Chaouat@onera.fr

<sup>1</sup> ONERA, 92322 Châtillon, France

## 1 Introduction

Different but complementary methods have been developed in the past fifty years for simulating turbulent flows. Obviously, direct numerical simulation (DNS) [1] solving all the scales on a mesh with a grid-size at least of order of magnitude of the Kolmogorov scale is the best tool for investigating turbulent flows. But this approach remains out of reach for all engineering applications. Large eddy simulation [1–3] (LES) which consists in modeling the more universal small scales while the large scales motions are explicitly computed is a promising route but remains also extremely costly in term of computer resources for domain with large dimension or at large Reynolds numbers, even with the rapid increase of supercomputer power [4–6]. For instance, an LES simulation of the flow around an entire aircraft still remains out of scope at present time. This problem is particularly acute at high Reynolds numbers since the Kolmogorov scale cubed decreases according to the Reynolds number  $R_t^{-9/4}$  power law of turbulence. Moreover, LES using eddy viscosity models (EVM) known as first-order models assuming a direct constitutive relation between the turbulence stress and strain components, cannot calculate the subgrid scale (SGS) turbulent energy and the subgrid scale stresses because these subgrid scale energies are not attainable in such models although they may be an appreciable part of the total energies. On the other hand, the Reynolds averaged Navier-Stokes (RANS) methodology based on a statistical averaging (or in practice a long-time averaging which is sufficiently large in comparison with the turbulence time scale [7]) including advanced eddy viscosity models (EVM), and Reynolds stress models (RSM) developed in the framework of second-moment closures (SMC) [3, 8, 9] appears well adapted for tackling engineering flows encountered in aeronautics applications with reasonable computational costs [10–12]. But although reaching a high level of sophistication in RANS methodology, RSM models may show some weaknesses in simulating turbulent flows in which the unsteady large scales play an important role. This happens in particular situations where the mean flow quantities are strongly affected by the dynamic of large scale turbulent eddies. As known, RANS models work well in flow situations where the time variations in the mean flow are of much lower frequency than the turbulence itself. This is the favored field of application of RANS and unsteady RANS (URANS). For these reasons, inability of RANS to reproduce unsteady flows and high computational costs for LES, new methods of turbulence modeling that combine the advantages of both RANS and LES methods have been recently proposed to simulate engineering or industrial flows [13]. They are essentially based on hybrid zonal methods but non-zonal methods have also emerged recently [14]. In this framework, different hybrid RANS/LES methods such as the very large eddy simulation (VLES) [15, 16], the detached eddy simulation (DES) [17–25], the partially integrated transport modeling (PITM) method [26–36], the partially averaged Navier-Stokes (PANS) method, [37–45], and the scale adaptive simulation (SAS) [46–48], have been developed for tackling these identified challenges. According to the literature [49–51], these hybrid methods can be classified into two categories, zonal and non-zonal methods. RANS/LES zonal methods rely on two different models, a RANS model and a subgrid-scale model, which are applied in different domains separated by a sharp or dynamic interface whereas non-zonal methods assume that the governing set of equations is smoothly transitioning from a RANS behavior to an LES behavior, based on criteria updated during the computation.

The objective of this paper is to present the state of the art at the present time of hybrid RANS/LES modeling for the simulation of turbulent flows. We will begin to analyze the RANS and LES methodologies and the way to unify these approaches with respect to their basic foundations by a theoretical method developed in the spectral space. Then, considering

these various hybrid RANS/LES methods that have been developed often independently from each other using theoretical or empirical arguments, we will investigate the principal hybrid methods that are currently used from a physical point of view. In particular, we will focus attention on VLES, DES, PITM, PANS and SAS methods. We will see that it is possible to establish a link between several methods, from one hand, PITM and PANS and from the other hand, DES and PITM, provided some assumptions are however made.

## 2 DNS

### 2.1 Navier-Stokes equations

The Navier-Stokes equations governing the detailed flow evolution are the starting point of the analysis. The equations of conservation of mass and momentum are

$$\frac{\partial u_j}{\partial x_j} = 0 \quad (1)$$

and

$$\frac{\partial u_i}{\partial t} + \frac{\partial}{\partial x_j}(u_i u_j) = -\frac{1}{\rho} \frac{\partial p}{\partial x_i} + \nu \frac{\partial^2 u_i}{\partial x_j \partial x_j} \quad (2)$$

where in this equation, the variables  $u_i$ ,  $p$  and  $\nu$  denote the velocity, pressure and molecular viscosity, respectively.

### 2.2 Computational resources for DNS

A direct numerical simulation [52–55] consists in solving all essential scales of motion that are at least of order of magnitude of the Kolmogorov scale  $\eta_K$  computed as  $\eta_K = (v^3/\epsilon)^{1/4}$  where  $\epsilon$  denotes the dissipation-rate. As a rough guide, in order to describe a “minimal” sine curve on a full period, the number of grid-points of the mesh is then given by

$$N_\eta = \frac{64 L^3}{\eta_K^3} \quad (3)$$

where  $L$  is the size of the computational domain. Considering a turbulent flow at the Reynolds number  $Re = U_b L/\nu$  based on the bulk velocity  $U_b$  and the characteristic length-scale  $L$ , Eq. 3 can be easily simplified if one considers that the size of the energetic big eddies  $L_e = k^{3/2}/\epsilon$  is roughly of order of magnitude of the characteristic geometrical size of the flow itself leading to  $N_\eta = 64 R_t^{9/4}$  where the turbulent Reynolds number is defined by  $R_t = L_e \sqrt{k}/\nu = (L_e/\eta_K)^{4/3} = k^2/(\nu\epsilon)$ . The computational time can be estimated if we assume that the turbulent Reynolds number is proportional to the mean flow Reynolds number  $R_t = \zeta Re$ , where  $\zeta$  is an empirical coefficient usually close to 1/10 in confined flows (and in usual Reynolds numbers range). It is then proportional to the Reynolds number according to the law  $t \propto 64\zeta R_t^{11/4}$ . These numerical order of magnitudes clearly show that DNS (or even highly resolved LES) implies a huge numerical task and still remains difficult to reach in practice at the present time even if considering the Moore’s law suggesting that the number of transistors of a processor doubles every second years (10 years = factor 32) and supercomputers as indicated in Table 1. The Moore’s prediction proved accurate for several decades. The rate of advancement was 22 nanometer feature width in 2012, 14 nm in 2015 and should be 10 nm in 2018. The projection suggests the same trend until 2025-2030 but it cannot be sustained indefinitely for technological reasons linked to the fundamental

**Table 1** List of supercomputers (Top500 November 2016) (<https://www.top500.org/lists/2016/11/>)

| RANK | SITE                            | SYSTEM                                       | CORES             | RPEAK (FLOPS/s)       |
|------|---------------------------------|--|-------------------|-----------------------|
| 1    | NSC Wuxi (China)<br>(2016)      | <b>Sunway TaihuLight</b> (1.45 GHz)<br>NRCPC | $10.6 \cdot 10^6$ | $125.4 \cdot 10^{15}$ |
| 2    | NSC Guangzhou (China)<br>(2013) | <b>Tianhe-2</b> (2.2 GHz)<br>NUDT            | $3.1 \cdot 10^6$  | $54.9 \cdot 10^{15}$  |
| 3    | DOE/SC/Oak (U.S.)<br>(2012)     | <b>Titan-Cray XK7</b> (2.2 GHz)<br>Cray Inc. | $0.5 \cdot 10^6$  | $27.1 \cdot 10^{15}$  |
| 4    | DOE/NNSA/LLNL (U.S.)<br>(2011)  | <b>Sequoia-BlueGene/Q</b> (1.6 GHz)<br>IBM   | $1.5 \cdot 10^6$  | $20.1 \cdot 10^{15}$  |
| 5    | DOE/NNSA/LLNL (U.S.)<br>(2016)  | <b>Cori-Cray XC40</b> (1.4 GHz)<br>Cray Inc. | $0.6 \cdot 10^6$  | $27.8 \cdot 10^{15}$  |

barrier of atoms. The exascale supercomputer ( $10^{18}$  floating point operations per second) is expected in 2020.

### 3 RANS Modeling

#### 3.1 Principle of the method

The RANS methodology is based on the Reynolds averaging in the statistical sense of the instantaneous Navier-Stokes equations. Applying the averaging process or in practice a long-time averaging that is sufficiently large in comparison with the turbulence time scale (and sufficiently small in comparison with the evolution time of the mean flow) on the instantaneous equations leads to the averaged equations of conservation of mass and momentum of the flow. As a result, the motion equation contains the unknown turbulent stress that must be modeled to close and solve the set of equations. This problem is known as the turbulence closure problem as described in detail in Refs. [8, 9, 56]. The turbulent stress is defined by the correlation of the fluctuating velocities including all the turbulence scales. The RANS method has been developed initially for simulating steady flows or flows that evolve slowly in time. The turbulent stress is modeled using eddy viscosity models or second moment closure models, depending of the level of closure considered. Usually, eddy viscosity models perform well for shear flows where the shear stress is the most important dynamical component of the stress tensor. Reynolds stress models account for more physics than eddy viscosity models and provide a better prediction of the normal turbulent stresses for flows encountered in aeronautical or turbomachinery applications where complex physics phenomena are produced by strong effects of streamline curvature such as detachment or reattachment of the boundary layer, separation and recirculation in presence of adverse pressure gradient, as well as rotational effects [7, 10–12, 57]. This modeling corresponds to the optimal level of closure for the prediction of turbulent flows.

#### 3.2 The averaging process

Turbulent flow of a viscous incompressible fluid is considered. The Reynolds averaged Navier-Stokes method in the statistical approach assumes that every instantaneous function

$\phi(\mathbf{x}, t)$  varying in time and space, can be decomposed into an ensemble average part  $\langle \phi \rangle$  and a fluctuating part that embodies all the turbulent scales  $\phi'$  such as  $\phi = \langle \phi \rangle + \phi'$ . From its definition, the statistical mean is defined as

$$\langle \phi(\mathbf{x}) \rangle = \lim_{N \rightarrow \infty} \frac{1}{N} \sum_{j=1}^N \phi_j(\mathbf{x}, t) \tag{4}$$

where  $\phi_j$  is the value associated with the  $j$  process and  $N$ , the total number of realizations of the flow. In practice, if assuming an ergodic assumption, the Reynolds averaging is obtained from time averaging over a sufficiently long period of time  $T$  in comparison with the characteristic turbulent time scale given itself by the ratio  $\tau = k/\epsilon$  where  $k$  denotes the turbulent energy. In the case where  $T \gg \tau$ , one gets

$$\langle \phi(\mathbf{x}) \rangle = \frac{1}{T} \int_0^T \phi(\mathbf{x}, t) dt \tag{5}$$

This approximation cannot be used in unsteady turbulent flows in the mean, except in the particular case of periodic flows in which phase averaging can be used. In most theoretical studies, the mean value is given by statistical averaging which allows a more consistent and general formalism in the turbulence equations.

### 3.3 Averaged equations

The transport equations of the mass conservation and the mean statistical velocity is obtained by applying the process (5) to Eqs. 1 and 2

$$\frac{\partial \langle u_j \rangle}{\partial x_j} = 0 \tag{6}$$

$$\frac{\partial \langle u_i \rangle}{\partial t} + \frac{\partial}{\partial x_j} (\langle u_i \rangle \langle u_j \rangle) = -\frac{1}{\rho} \frac{\partial \langle p \rangle}{\partial x_i} + \nu \frac{\partial^2 \langle u_i \rangle}{\partial x_j \partial x_j} - \frac{\partial R(u_i, u_j)}{\partial x_j} \tag{7}$$

where the Reynolds stress tensor  $R(u_i, u_i)$  is defined as

$$R(u_i, u_j) = R_{ij} = \langle u_i u_i \rangle - \langle u_i \rangle \langle u_j \rangle \tag{8}$$

The stress  $R_{ij}$  represents the effect of the turbulence scales on the mean field.

### 3.4 Closure of equations

#### 3.4.1 Eddy viscosity models

In the case of eddy viscosity models, the Reynolds stress tensor  $R_{ij}$  appearing in the right-hand side of Eq. 7 is modeled by means of the Boussinesq hypothesis, non-linear model or even algebraic stress model [58] taking into account an eddy viscosity. The Boussinesq hypothesis leads to the well known relation

$$R_{ij} = -2\nu_t \langle S_{ij} \rangle + \frac{2}{3} k \delta_{ij} \tag{9}$$

where  $\nu_t$  is the turbulent viscosity that must be modeled, and where  $S_{ij}$  denotes the strain deformation

$$S_{ij} = \frac{1}{2} \left( \frac{\partial u_i}{\partial x_j} + \frac{\partial u_j}{\partial x_i} \right) \tag{10}$$

The principal models in use are the model of Spalart-Allmaras (S-A) [59, 60] based on a single transport equation for the effective viscosity  $\tilde{\nu}$  allowing the computation of  $\nu_t$  and the two-equation models such as the  $k - \epsilon$  initially developed by Jones and Launder [61] considering the transport equations for the turbulent kinetic energy  $k$  and the dissipation-rate  $\epsilon$  or its variant  $k - \omega$  developed by Wilcox [62] using the characteristic frequency  $\omega = \epsilon / (c_\mu k)$  where  $c_\mu$  is a constant coefficient, as well as the shear-stress transport model (SST) developed by Menter [63] that is a combination of  $k - \epsilon$  and  $k - \omega$  models. The transport equation for the effective turbulent viscosity  $\tilde{\nu}$  in the model of Spalart and Allmaras especially developed for applications of aerodynamic flows is empirically built as follows [60]

$$\frac{\partial \tilde{\nu}}{\partial t} + \frac{\partial}{\partial x_j} (\tilde{\nu} \langle u_j \rangle) = C_{b1} \tilde{\nu} \tilde{S} + \frac{1}{\sigma} \left[ \frac{\partial}{\partial x_j} \left( (v + \tilde{\nu}) \frac{\partial \tilde{\nu}}{\partial x_j} \right) + C_{b2} \frac{\partial \tilde{\nu}}{\partial x_j} \frac{\partial \tilde{\nu}}{\partial x_j} \right] - C_{w1} f_w \frac{\tilde{\nu}^2}{d_w^2} \tag{11}$$

where the terms appearing in the right hand side of this equation are identified as production, diffusion and dissipation. The quantity  $\tilde{S}$  corresponds to the magnitude of the vorticity,  $d_w$  is the wall distance whereas the other parameters are coefficients or blending functions defined in the original paper [60]. The turbulent eddy viscosity is then deduced from  $\tilde{\nu}$  by the simple relation  $\nu_t = \tilde{\nu} f_{\nu 1}$  where  $f_{\nu 1}$  is a given function of the ratio  $\chi = \tilde{\nu} / \nu$  [60]. In the case of the  $k - \epsilon$  model, the turbulent eddy viscosity  $\nu_t$  is computed by means of the turbulent energy and dissipation-rate as

$$\nu_t = c_\mu \frac{k^2}{\epsilon} \tag{12}$$

where  $k$  and  $\epsilon$  are themselves computed by their own transport equations. At high Reynolds number, the modeled transport equation of the turbulent energy reads [61]

$$\frac{\partial k}{\partial t} + \frac{\partial}{\partial x_j} (k \langle u_j \rangle) = P - \epsilon + J_k \tag{13}$$

where the terms appearing in the right hand side of this equation are identified as the processes of production  $P$ , dissipation-rate  $\epsilon$  and diffusion  $J_k$ . The modeled transport equation of the dissipation-rate reads

$$\frac{\partial \epsilon}{\partial t} + \frac{\partial}{\partial x_j} (\epsilon \langle u_j \rangle) = c_{\epsilon 1} \frac{\epsilon}{k} P - c_{\epsilon 2} \frac{\epsilon^2}{k} + J_\epsilon \tag{14}$$

where  $c_{\epsilon 1}$  and  $c_{\epsilon 2}$  are constant coefficients. The production term  $P$  is given by

$$P = -R_{ij} \frac{\partial \langle u_j \rangle}{\partial x_i} \tag{15}$$

The turbulence diffusion terms  $J_k$  and  $J_\epsilon$  are modeled using a well known gradient law hypothesis

$$J_k = \frac{\partial}{\partial x_j} \left[ \left( \nu + \frac{\nu_t}{\sigma_k} \right) \frac{\partial k}{\partial x_j} \right] \tag{16}$$

and

$$J_\epsilon = \frac{\partial}{\partial x_j} \left[ \left( \nu + \frac{\nu_t}{\sigma_\epsilon} \right) \frac{\partial \epsilon}{\partial x_j} \right] \tag{17}$$

where  $\sigma_k$  and  $\sigma_\epsilon$  are constant coefficients. In low Reynolds number flows, additional correction terms may also appear in Eq. 14, but they are not detailed here. In the case of the two equation  $k - \omega$  model [62], the transport equations for  $k$  and  $\omega$  read formally

$$\frac{\partial k}{\partial t} + \frac{\partial}{\partial x_j} (k \langle u_j \rangle) = P - \beta^* \omega k + J'_k \tag{18}$$

$$\frac{\partial \omega}{\partial t} + \frac{\partial}{\partial x_j} (\omega \langle u_j \rangle) = \frac{\gamma}{v_t} P - \beta^* \omega^2 + J_\omega \tag{19}$$

where  $\gamma$  and  $\beta^*$  are coefficients,  $J'_k$  and  $J_\omega$  denote the diffusion processes. In this model, the turbulent eddy viscosity is computed as  $\nu_t = k/\omega = C_\mu k^2/\epsilon$ .

### 3.4.2 Reynolds stress models

Second moment closure is a more advanced turbulence modeling [8, 9] developed initially by Hanjalic and Launder [64], Launder et al. [65]. The modeled transport equation of the turbulent stress  $R_{ij}$  can be written in a compact form as

$$\frac{\partial R_{ij}}{\partial t} + \frac{\partial}{\partial x_k} (R_{ij} \langle u_k \rangle) = P_{ij} + \Pi_{ij} - \epsilon_{ij} + J_{ij} \tag{20}$$

where in this equation, the production term  $P_{ij}$  takes on the exact expression

$$P_{ij} = -R_{ik} \frac{\partial \langle u_j \rangle}{\partial x_k} - R_{jk} \frac{\partial \langle u_i \rangle}{\partial x_k} \tag{21}$$

The redistribution term  $\Pi_{ij}$  is usually decomposed into a slow part  $\Pi_{ij}^1$  which characterizes the return to isotropy due to the action of turbulence on itself and a rapid part  $\Pi_{ij}^2$  which describes the return to isotropy by action of the mean velocity gradient [64–66]. In a first approach, these terms are modeled as

$$\Pi_{ij}^1 = -c_1 \frac{\epsilon}{k} \left( R_{ij} - \frac{2}{3} k \delta_{ij} \right) \tag{22}$$

where  $c_1$  is the constant Rotta coefficient. The second term  $\Pi_{ij}^2$  is modeled by means of the rapid distortion theory (RDT) for homogeneous strained turbulence in an initially isotropic state [67]

$$\Pi_{ij}^2 = -c_2 \left( P_{ij} - \frac{1}{3} P_{mm} \delta_{ij} \right) \tag{23}$$

where the coefficient  $c_2$  is a constant coefficient. The dissipation-rate  $\epsilon_{ij}$  is usually modeled at high Reynolds number assuming that the small scales are isotropic  $\epsilon_{ij} = 2/3 \delta_{ij} \epsilon$ . The diffusion term  $J_{ij}$  appearing in Eq. 20 associated with the fluctuating velocities and pressure together with the molecular diffusion is modeled assuming a well known gradient law hypothesis

$$J_{ij} = \frac{\partial}{\partial x_k} \left( v \frac{\partial R_{ij}}{\partial x_k} + c_s \frac{k}{\epsilon} R_{kl} \frac{\partial R_{ij}}{\partial x_l} \right) \tag{24}$$

where  $c_s$  is a constant coefficient. The dissipation-rate  $\epsilon$  is computed from its modeled transport given by Eq. 14 but the diffusion term is modeled by means of a tensorial eddy viscosity concept as follows

$$J_\epsilon = \frac{\partial}{\partial x_j} \left( v \frac{\partial \epsilon}{\partial x_j} + c_\epsilon \frac{k}{\epsilon} R_{jm} \frac{\partial \epsilon}{\partial x_m} \right) \tag{25}$$

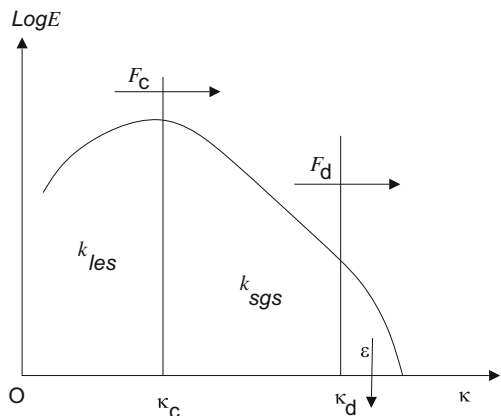
where the coefficient  $c_\epsilon$  is a constant coefficient. More advanced turbulence modeling use in SMC can be found in Refs. [57, 68, 69].

## 4 Large Eddy Simulation

### 4.1 Principle of the method

Large-Eddy Simulation (LES) [1–3] is a promising route towards the calculation of turbulent flows which has been now largely developed [70, 71] and relies on the spectral filtering of turbulence energy, the most suggestive type of filtering being the spectral splitting as sketched in Fig. 1. The energy spectrum [72] is then decomposed into different zones with respect to the cutoff wave number  $\kappa_c$  given itself by the grid size  $\Delta$  as  $\kappa_c = \pi/\Delta$ , and the dissipative wave number  $\kappa_d$  located at the far end of the inertial range of the spectrum assuming that the energy pertaining to higher wave numbers is negligible. Turbulent energy is transferred from the large scales to the small scales by the turbulence cascade involving non-linear interactions although backscatter of energy is possible [1–3]. The spectral fluxes corresponding to the wave numbers  $\kappa_c$  and  $\kappa_d$  are denoted  $F_c$  and  $F_d$ , respectively. The LES method consists in modeling the more isotropic small-scales of the energy spectrum  $E(\kappa)$  for  $\kappa > \kappa_c$  while the large scales motions are explicitly calculated. This technique assumes that the filter cutoff occurs at a wave number which is located in the inertial range of the spectrum given by  $E(\kappa) = C_K \epsilon^{2/3} \kappa^{-5/3}$  (located before  $\kappa_d$ ) where  $C_K$  is the Kolmogorov constant. LES thus appears as a good compromise between DNS which resolves all the turbulent scales and RANS statistical modeling in which the whole flow structures are modeled. Contrary to full statistical modeling, LES enables to mimic the mechanisms of turbulent interactions, and information on velocity, pressure fluctuations and two-point correlations are possible to obtain. Applying the filtering process on the instantaneous equations leads to the filtered equations of conservation of mass and momentum of the flow where the turbulent subgrid scale stress must be modeled to close the system of equations. In the past, the most widely used subgrid-scale model was a viscosity type model proposed by Smagorinsky (SM) [73]. It is based on an implicit equilibrium hypothesis which assumes that the viscosity can be calculated using the resolved scales as a characteristic velocity and the grid size as a characteristic length. Many flow studies can be found in the scientific literature that have used this model. However, it soon appeared that the Smagorinsky constant is not universal and must be varied from one flow to another. New trends in LES of turbulence have been proposed in the past two decades [70] including for instance the dynamic Smagorinsky model (DSM) [74, 75] or the structure function model (SFM) [76].

**Fig. 1** Sketch of spectral splitting of turbulence energy in LES





Eddy viscosity models based on the transport equation of the subgrid scale turbulent energy [77–79] or second moment closure models based on the transport equation of the subgrid scale stresses [80, 81], both levels of closure using an algebraic relation for length-scale, have been also proposed to overcome the limitations of the Smagorinsky type model. Large eddy simulation that accurately resolves the viscous region of wall-bounded flows is very costly in computer time because of the very refined mesh near the wall that increases the number of grid points and leads also to a reduction of the Courant-Friedrichs-Lewy (CFL) number selected in the simulation. As a consequence, the extension of LES to practical applications is not always feasible with reasonable computational resources. For this reason, several techniques have been proposed to model the wall flow region instead of solving all the turbulent scales [82–85]. LES is then performed in the core flow accounting for a wall modeling (WM) for reproducing the boundary layer. The first technique is based on the equilibrium laws [77] assuming a relation between the shear stress at the wall and the velocity of the core flow and was afterwards improved to take into account the inclination of the elongated structures in the near wall region [82]. The second technique relies on a zonal approach based on the explicit solution of a different set of equations in the inner layer [82]. In this framework, there are two different approaches. The first one uses two wall layers (TLM) with two different calculation grids [86] whereas the second one uses a single calculation grid as in DES [17].

### 4.2 Filtering process

In large eddy simulations, the variable  $\phi$  is decomposed into a large scale (or resolved part)  $\bar{\phi}$  and a subfilter-scale (SFS) fluctuating part  $\phi^>$  or modeled part such that  $\phi = \bar{\phi} + \phi^>$ . The filtered variable  $\bar{\phi}$  is defined by the filtering operation as the convolution with a filter  $G$  in physical space

$$\bar{\phi} = G * \phi \tag{26}$$

that leads to the computation of a variable convolution integral

$$\bar{\phi}(\mathbf{x}, t) = \int_{\mathbb{R}^3} G[\mathbf{x} - \boldsymbol{\xi}, \Delta(\mathbf{x}, t)] \phi(\boldsymbol{\xi}, t) d\boldsymbol{\xi} \tag{27}$$

The instantaneous fluctuation  $\phi'$  appearing in RANS methodology contains in fact the large scale fluctuating part  $\phi^<$  and the small scale fluctuating part  $\phi^>$  such that  $\phi' = \phi^< + \phi^>$ . So that the instantaneous variable  $\phi$  can then be rewritten like the sum of a mean statistical part  $\langle \phi \rangle$ , a large scale fluctuating part  $\phi^<$  and a small scale fluctuating part  $\phi^>$  as follows  $\phi = \langle \phi \rangle + \phi^< + \phi^>$ . As made in Ref. [28], in the framework of spectral splitting, it is possible to define the large scale fluctuations (resolved scales)  $\phi^<$  and the fine scales (modeled scales)  $\phi^>$  through the relations

$$\phi^< = \int_{|\boldsymbol{\kappa}| \leq \boldsymbol{\kappa}_c} \widehat{\phi}'(\boldsymbol{\kappa}) \exp(j\boldsymbol{\kappa}\boldsymbol{\xi}) d\boldsymbol{\kappa} \tag{28}$$

and

$$\phi^> = \int_{|\boldsymbol{\kappa}| \geq \boldsymbol{\kappa}_c} \widehat{\phi}'(\boldsymbol{\kappa}) \exp(j\boldsymbol{\kappa}\boldsymbol{\xi}) d\boldsymbol{\kappa} \tag{29}$$

where  $\widehat{\phi}$  denotes the Fourier transform of  $\phi$  and  $\boldsymbol{\kappa}_c$  is the cutoff wave vector verifying  $|\boldsymbol{\kappa}_c| = \boldsymbol{\kappa}_c = \pi/\Delta$ . This particular filter, as a spectral truncation, presents some interesting properties that are not possible with continuous filters. In particular, it can be shown [87, 88] that large scale and small scale fluctuations are uncorrelated  $\langle \phi^> \phi^< \rangle = 0$ . The most commonly used filters in the physical space are the box and Gaussian filters. Using the

definition (27), it is obvious to see that the Fourier transform of the filtered variable  $\bar{\phi}$  in homogeneous turbulence is simply

$$\widehat{\bar{\phi}}(\boldsymbol{\kappa}, t) = \widehat{G}(\boldsymbol{\kappa}, \boldsymbol{\kappa}_c) \widehat{\phi}(\boldsymbol{\kappa}, t) \tag{30}$$

If in the spectral space, the filtering operation is naturally defined by the spectral cutoff wave number, the interpretation in the physical space by inverse Fourier transform however leads in this case to some complexities because of the more intricate form of the filter function [33, 89].

### 4.3 Filtered equations

Due to the fact that the filtering operation does not commute with the space or time derivative, commutation terms appear in the derivative in space  $\partial\bar{\phi}/\partial x_i$  or in time  $\partial\bar{\phi}/\partial t$  such as [33, 90]

$$\frac{\partial\bar{\phi}}{\partial x_i}(\mathbf{x}, t) = \overline{\frac{\partial\phi}{\partial x_i}}(\mathbf{x}, t) + \frac{\partial\Delta}{\partial x_i} \frac{\partial\bar{\phi}}{\partial\Delta}(\mathbf{x}, t) \tag{31}$$

and equivalently, if transposing (31) in time for the derivative  $\partial\bar{\phi}/\partial t$

$$\frac{\partial\bar{\phi}}{\partial t}(\mathbf{x}, t) = \overline{\frac{\partial\phi}{\partial t}}(\mathbf{x}, t) + \frac{\partial\Delta}{\partial t} \frac{\partial\bar{\phi}}{\partial\Delta}(\mathbf{x}, t) \tag{32}$$

Using Eqs. 31 and 32, it simple matter to show that

$$\frac{d\bar{\phi}}{dt} = \frac{\partial\bar{\phi}}{\partial t} + \frac{\partial(\bar{u}_j\bar{\phi})}{\partial x_j} + \frac{\partial\tau(u_j, \phi)}{\partial x_j} - \beta_T(\phi) \tag{33}$$

where  $\beta_T(\phi) = \beta_t(\phi) + \beta_{x_j}(u_j\phi)$  with

$$\beta_t(\phi) = \frac{\partial\Delta}{\partial t} \frac{\partial\bar{\phi}}{\partial\Delta} \tag{34}$$

$$\beta_{x_j}(u_j\phi) = \frac{\partial\Delta}{\partial x_j} \frac{\partial}{\partial\Delta} (\bar{u}_j\bar{\phi} + \tau(u_j, \phi)) \tag{35}$$

where  $\tau(u_j, \phi)$  is a function defined as

$$\tau(u_j, \phi) = \overline{u_j\phi} - \bar{u}_j\bar{\phi} \tag{36}$$

The transposition in space of Eq. 34 is

$$\beta_{x_i}(\phi) = \frac{\partial\Delta}{\partial x_i} \frac{\partial\bar{\phi}}{\partial\Delta} \tag{37}$$

As a result, Eq. 33 including  $\beta_T$  is used to derive the filtered Navier-Stokes equations. The filtered equation of mass conservation reads

$$\frac{\partial\bar{u}_j}{\partial x_j} - \beta_{x_j}(u_j) = 0 \tag{38}$$

while the filtered motion equation is obtained using Eq. 33

$$\begin{aligned} \frac{\partial\bar{u}_i}{\partial t} + \frac{\partial(\bar{u}_i\bar{u}_j)}{\partial x_j} - \beta_T(u_i) &= -\frac{1}{\rho} \frac{\partial\bar{p}}{\partial x_i} + \frac{1}{\rho} \beta_{x_i}(p) - \frac{\partial\tau(u_i, u_j)}{\partial x_j} \\ + \nu \frac{\partial^2\bar{u}_i}{\partial x_j\partial x_j} - \nu \frac{\partial^2\Delta}{\partial x_j\partial x_j} \frac{\partial\bar{u}_i}{\partial\Delta} - \nu \frac{\partial\Delta}{\partial x_j} \frac{\partial\Delta}{\partial x_j} \frac{\partial^2\bar{u}_i}{\partial\Delta^2} - 2\nu \frac{\partial\Delta}{\partial x_j} \frac{\partial^2\bar{u}_i}{\partial x_j\partial\Delta} \end{aligned} \tag{39}$$

The presence of the subfilter scale stress

$$\tau(u_i, u_j) = (\tau_{ij})_{sfs} = \overline{u_i u_j} - \bar{u}_i \bar{u}_j \tag{40}$$

in Eq. 39 represents the effect of the subfilter turbulence scales on the resolved field. The subfilter scale tensor  $(\tau_{ij})_{sfs}$  can be historically developed into several contributions including the Leonard stresses, cross terms and small scales fluctuating velocity correlations as [91]

$$(\tau_{ij})_{sfs} = [\overline{\bar{u}_i \bar{u}_j} - \bar{u}_i \bar{u}_j] + [\overline{u_i^> u_j^>} + \overline{u_i^> \bar{u}_j}] + \overline{u_i^> u_j^>} \tag{41}$$

but this decomposition is no longer retained in LES because  $(\tau_{ij})_{sfs}$  is now modeled as a whole. Similarly, the resolved scale tensor is defined by the relation

$$\tau_r(u_i, u_j) = (\tau_{ij})_{les} = \bar{u}_i \bar{u}_j - \langle u_i \rangle \langle u_j \rangle \tag{42}$$

It is simple matter to show that  $\langle \tau(u_i, u_j) \rangle = \langle u_i^> u_j^> \rangle$  and  $\langle \tau_r(u_i, u_j) \rangle = \langle u_i^< u_j^< \rangle$ . Using the decomposition  $\phi = \langle \phi \rangle + \phi^< + \phi^>$ , the Reynolds stress tensor  $R_{ij}$  from Eq. 8 is given by

$$R_{ij} = \langle u_i^< u_j^< \rangle + \langle u_i^> u_j^> \rangle + \langle u_i^< u_j^> \rangle + \langle u_i^> u_j^< \rangle \tag{43}$$

So that, assuming that the correlation between the small scale and large scale  $\langle u_i^< u_j^> \rangle$  are small compared to the other correlations,  $R_{ij}$  can be computed in a first approximation as the sum of the statistical average of subfilter and resolved stresses

$$R_{ij} \approx \langle (\tau_{ij})_{sfs} \rangle + \langle (\tau_{ij})_{les} \rangle \tag{44}$$

Strictly speaking, the filtered (38) and (39) do not satisfy the conservation of mass and momentum as the RANS equations because of the commutation terms that appear in these equations. But if we assume that the commutation terms are negligible, we can see that the RANS and LES motion equations take exactly the same mathematical form [92, 93]. This is the main argument that allows to build hybrid RANS/LES methods. The difference between the RANS and LES methodologies relies only on the closure of equations. Indeed, in RANS, the closure is made by means of the flow variables, while in LES, it is worked out by considering both the flow variable and the grid size  $\Delta$  of the mesh (in fact, the filter width) involving the cutoff wave number  $\kappa_c$  of the energy spectrum.

### 4.4 Closure of equations

#### 4.4.1 Eddy viscosity models

Eddy viscosity models include the Smagorinsky model [73], already cited, or in its dynamic version, the dynamic subgrid-scale eddy viscosity model [74] but also other models based on transport equation for the subgrid turbulent energy [77–79, 94]. In the case of subgrid-scale eddy viscosity models involving the grid size  $\Delta$ , the subgrid scale stress tensor  $(\tau_{ij})_{sgs}$  appearing in the right-hand side of Eq. 39 is modeled by means of the Boussinesq hypothesis, non-linear model or even algebraic stress model. As for Eq. 9, the Boussinesq assumption in LES leads to

$$(\tau_{ij})_{sgs} = -2\nu_{sgs} \bar{S}_{ij} + \frac{2}{3} k_{sgs} \delta_{ij} \tag{45}$$

where the subgrid turbulent eddy viscosity must be modeled. In the case of the well known Smagorinsky model inspired by the mixing length hypothesis, the eddy viscosity is computed by

$$\nu_{sgs} = (C_s \Delta)^2 \sqrt{2\bar{S}_{ij}\bar{S}_{ij}} \tag{46}$$

where  $C_s$  is the Smagorinsky coefficient that takes on a constant value [73] or a variable coefficient evaluated locally and dynamically in space using a second test filter [74, 75]. In the case of one transport equation for the subgrid turbulent energy  $k_{sgs} = (\tau_{ii})_{sgs}/2$ , the turbulent viscosity  $\nu_{sgs}$  is obtained by

$$\nu_{sgs} = c_\mu k_{sgs}^{1/2} \Delta \tag{47}$$

where  $\Delta$  is the grid size of the mesh. In first moment closure, the subfilter energy  $k_{sgs}$  is computed by means of its transport equation. The modeling of the subgrid energy equation has been worked out by several authors such as Schumann, Yoshizawa and Horiuti [77–79]. This one is inspired from its corresponding RANS modeling but assumes that the turbulence length-scale is of the same order of the grid-size  $\Delta$  leading to

$$\frac{\partial k_{sgs}}{\partial t} + \frac{\partial}{\partial x_j} (k_{sgs} \bar{u}_j) = P_{sgs} - \epsilon_{sgs} + (J_k)_{sgs} \tag{48}$$

where  $P_{sgs}$ ,  $\epsilon_{sgs}$  and  $(J_k)_{sgs}$  denote the production, dissipation-rate and diffusion terms, respectively. The production term is given by

$$P_{sgs} = -(\tau_{ij})_{sgs} \frac{\partial \bar{u}_j}{\partial x_i} \tag{49}$$

The modeling of the dissipation-rate is then not given by its transport equation as in RANS modeling but it is then explicitly computed by means of the grid size  $\Delta$  as

$$\epsilon_{sgs} = C_\epsilon \frac{k_{sgs}^{3/2}}{\Delta} \tag{50}$$

where  $C_\epsilon$  is a constant coefficient. The diffusion term is modeled by analogy with the RANS modeling as

$$(J_k)_{sgs} = \frac{\partial}{\partial x_j} \left[ \left( \nu + \frac{\nu_{sgs}}{\sigma_k} \right) \frac{\partial k_{sgs}}{\partial x_j} \right] \tag{51}$$

where  $\sigma_k$  is a constant coefficient.

#### 4.4.2 Subgrid scale stress models

In the case of second moment closure, the turbulent subgrid scale  $(\tau_{ij})_{sgs} = \tau(u_i, u_j)$  is computed by means of its transport equation with a closure for the dissipation-rate given by Eq. 50. One of the first subgrid scale stress model was derived by Deardorff [80, 81] considering the transport equation for the correlation of the subgrid-scale fluctuating velocities  $\overline{u_i^> u_j^>}$  appearing in Eq. 41. The modeled equation reads

$$\frac{\partial (\tau_{ij})_{sgs}}{\partial t} + \frac{\partial}{\partial x_k} ((\tau_{ij})_{sgs} \bar{u}_k) = (P_{ij})_{sgs} + (\Pi_{ij})_{sgs} - \frac{2}{3} \delta_{ij} \epsilon_{sgs} + (J_{ij})_{sgs} \tag{52}$$

where in this equation, the production term  $(P_{ij})_{sgs}$  takes on the exact expression

$$(P_{ij})_{sgs} = -(\tau_{ik})_{sgs} \frac{\partial \bar{u}_j}{\partial x_k} - (\tau_{jk})_{sgs} \frac{\partial \bar{u}_i}{\partial x_k} \tag{53}$$

The redistribution term  $(\Pi_{ij})_{sgs}$  appearing in Eq. 52 is modeled considering the analogy between the RANS and LES modeling assuming that the interaction mechanisms of the

subgrid scales with the resolved scales of the turbulence is of the same nature than the interaction mechanisms involving all the fluctuating scales with the main flow. The redistribution term  $(\Pi_{ij})_{sgs}$  is then given by

$$\Pi_{ij}^1 = -c_m \frac{k_{sgs}^{1/2}}{\Delta} \left( (\tau_{ij})_{sgs} - \frac{2}{3} k_{sgs} \delta_{ij} \right) \tag{54}$$

where  $c_m$  is a constant coefficient that plays the same role as the Rotta coefficient. The second term  $(\Pi_{ij}^2)_{sgs}$  is modeled by means of the rapid distortion theory (RDT) for homogeneous strained turbulence in an initially isotropic state [66, 67]

$$\left( \Pi_{ij}^2 \right)_{sgs} = \frac{2}{5} k_{sgs} \bar{S}_{ij} \tag{55}$$

Equation 55 can be recovered from Eq. 23 in the particular case of isotropic turbulence for the coefficient value  $c_2 = 3/5$ . The diffusion term  $(J_{ij})_{sgs}$  appearing in Eq. 52 is modeled by means of the gradient law hypothesis [95]

$$(J_{ij})_{sgs} = \frac{\partial}{\partial x_k} \left[ c_m \Delta k_{sgs}^{1/2} \left( \frac{\partial (\tau_{ij})_{sgs}}{\partial x_k} + \frac{\partial (\tau_{ik})_{sgs}}{\partial x_j} + \frac{\partial (\tau_{jk})_{sgs}}{\partial x_i} \right) \right] \tag{56}$$

where  $c_m$  is a constant coefficient. Some justification for the assumptions and the way in which the constants are evaluated are given in Ref. [80]. This model was originally applied for the simulation of three-dimensional atmospheric turbulence [80, 81].

## 5 A Theoretical Formalism to Unify RANS and LES Methods

### 5.1 General properties

As emerge from the previous considerations, although RANS and LES approaches both lead to very similar evolution equations of motion, they rely on different grounds, statistical average for RANS and filtering for LES. The development of hybrid methods needs to bridge the RANS and LES methodologies not only from a practical point of view but also from a theoretical point of view. So, considering the numerous turbulence models used in RANS and LES that have been developed often independently from each other, it seems of primary importance to unify these different methodologies, referring to their basic physical foundations, with the aim of building hybrid RANS/LES models. It has been shown in Ref. [28] that spectral turbulence theory can provide the main ingredient of this development [28]. The theory deals with the dynamic equation of the two-point fluctuating velocity correlations with extensions to the case of nonhomogeneous flows. This choice is motivated by the fact that the two-point velocity correlation equation enables a detailed description of the turbulence field that also contains the one point information as a special case. By using Fourier transform and performing averaging on spherical shells on the dynamic equation, one can formally obtain the evolution equation of the spectral velocity correlation tensor in one-dimensional spectral space [96–99]. On the one hand, a full integration over the wave number space of the resulting evolution equation of the spectral velocity correlation tensor allows to recover formally usual one-point statistical models. On the other hand, a partial integration over a split spectrum, with a given spectral partitioning, yields partial integrated transport models that can be transposed both in statistical multiple-scale models [98, 100], or in large eddy simulations [26, 27]. In the present case, any flow variable  $\phi$  is decomposed

into a statistical mean value and a fluctuating turbulent part which may be developed into several ranks of fluctuating parts using an extension of the Reynolds decomposition [98]

$$\phi = \langle \phi \rangle + \sum_{m=1}^{\infty} \phi'_{[\kappa_{m-1}, \kappa_m]} \tag{57}$$

where the partial fluctuating velocities are defined by partial integration of their generalized Fourier transform

$$\phi'_{[\kappa_{m-1}, \kappa_m]}(\xi) = \int_{\kappa_{m-1} < |\kappa| < \kappa_m} \widehat{\phi}'(\kappa) \exp(j\kappa\xi) d\kappa, \tag{58}$$

where  $\widehat{\phi}'(\kappa)$  denotes the Fourier transform of  $\phi'(\xi)$  and  $\kappa_m$  is a series of partitioning (possibly evolving) wave numbers. Applying the basic decomposition of the turbulent velocity defined by relations (57) and (58) for  $m = 1$  allows to recover the Reynolds velocity decomposition  $\phi = \langle \phi \rangle + \phi'_{[0, \infty]}$  used in RANS models in which the whole spectrum is modeled. For  $m = 2$  or higher, we find the usual decomposition retained for the multiple-scale statistical models [98]. The two-level decomposition  $m = 2$  is also relevant for the decomposition used in large eddy simulations where only one part of the spectrum containing the small eddies is modeled  $\phi = \langle \phi \rangle + \phi^< + \phi^>$  with  $\phi^< = \phi'_{[0, \kappa_1]}$  and  $\phi^> = \phi'_{[\kappa_c, \kappa_2]}$  whereas the other part of the spectrum containing large eddies is resolved by the simulation. In this framework,  $\kappa_1$  denotes the cutoff wave number  $\kappa_c$  whereas  $\kappa_2$  is the dissipative wave number  $\kappa_d$ .

### 5.2 Transport equation of the two-point velocity fluctuation

The general case of nonisotropic inhomogeneous turbulence is considered for bridging the gap between the RANS and LES methodologies. In this case, the two-point velocity correlation  $R_{ij} = \langle u'_{iA} u'_{jB} \rangle$  is function of the distance between the points  $A$  and  $B$ , denoted  $\xi$ , but also of the location of these points  $\mathbf{x}_A$  and  $\mathbf{x}_B$  in the flow field because of the inhomogeneity of the turbulence field. New independent variables defined by the vector difference  $\xi = \mathbf{x}_B - \mathbf{x}_A$  and the midway position  $\mathbf{X} = \frac{1}{2}(\mathbf{x}_A + \mathbf{x}_B)$  are then considered in order to distinguish the effects of the distance separation from the effects of space location [72] so that each variable can be regarded as a function of the two variables  $\xi$  and  $\mathbf{X}$ . The first step is to write the dynamic equation for the double velocity correlation that reads [28]

$$\begin{aligned} & \frac{\partial R_{ij}(\mathbf{X}, \xi, t)}{\partial t} + \langle u_k \rangle(\mathbf{X}) \frac{\partial R_{ij}(\mathbf{X}, \xi, t)}{\partial X_k} \\ &= -R_{jk}(\mathbf{X}, \xi, t) \frac{\partial \langle u_i \rangle}{\partial X_k} - R_{ik}(\mathbf{X}, \xi, t) \frac{\partial \langle u_j \rangle}{\partial X_k} - \xi_p \frac{\partial \langle u_k \rangle}{\partial X_p} \frac{\partial R_{ij}}{\partial \xi_k}(\mathbf{X}, \xi, t) \\ & \quad - \frac{1}{2} \frac{\partial}{\partial X_k} (S_{i,kj} + S_{ik,j})(\mathbf{X}, \xi, t) - \frac{\partial}{\partial \xi_k} (S_{i,kj} - S_{ik,j})(\mathbf{X}, \xi, t) \\ & \quad - \frac{1}{2\rho} \left( \frac{\partial K_{(p)j}}{\partial X_i} + \frac{\partial K_{i(p)}}{\partial X_j} \right) (\mathbf{X}, \xi, t) + \frac{1}{\rho} \left( \frac{\partial K_{(p)j}}{\partial \xi_i} - \frac{\partial K_{i(p)}}{\partial \xi_j} \right) (\mathbf{X}, \xi, t) \\ & \quad + \frac{\nu}{2} \frac{\partial^2 R_{ij}(\mathbf{X}, \xi, t)}{\partial X_l \partial X_l} + 2\nu \frac{\partial^2 R_{ij}(\mathbf{X}, \xi, t)}{\partial \xi_l \partial \xi_l} \end{aligned} \tag{59}$$

where the term  $S_{i,jk}$  and  $S_{ik,j}$  denote the turbulent diffusion terms due to the fluctuating velocities  $S_{i,kj}(\mathbf{X}, \xi, t) = \langle u'_{iA} u'_{kB} u'_{jB} \rangle$ ,  $S_{ik,j}(\mathbf{X}, \xi, t) = \langle u'_{iA} u'_{kA} u'_{jB} \rangle$  and the terms  $K_{(p)i}$  and  $K_{i(p)}$  are turbulent diffusion terms due to the fluctuating pressure defined by

$K_{(p)i}(X, \xi, t) = \langle p'_A u'_{iB} \rangle$ , and  $K_{i(p)}(X, \xi, t) = \langle p'_B u'_{iA} \rangle$ . Equation 59 is written in this form to give a direct connection with the one-point Reynolds stress equation [96, 98]. Indeed, the nonhomogeneous terms appearing in Eq. 59 correspond to the usual terms in one-point equation whereas the others terms involving the distance  $\xi$  are treated as in homogeneous anisotropic turbulence. This formalism leads to consider the tangent homogeneous anisotropic field at point  $X$  of the nonhomogeneous field implying that the variation of the mean velocities is accounted for by the use of Taylor series expansion in space limited to the linear terms. This concept ensures that the filtered field goes to the statistical mean field when the filter width goes to infinity ( $\Delta \rightarrow \infty$ ,  $\kappa_c \rightarrow 0$  and  $\bar{\phi} \rightarrow \langle \phi \rangle$ ). In particular, when the cutoff vanishes, the full integration in the tangent homogeneous space exactly corresponds to the statistical mean, that guarantees exact compatibility with RANS equations [28]. The second step consists in taking the Fourier transform of Eq. 59 using the definition

$$\widehat{\phi}(X, \kappa) = \int \phi(X, \xi) \exp(-j\kappa\xi) d\xi \tag{60}$$

### 5.3 One-dimensional models by spherical mean

In the third step, we apply on the variable  $\widehat{\phi}(X, \kappa)$  the spherical mean operator  $(.)^\Delta$  defined in Refs. [96–99]

$$[\phi(X)]^\Delta(\kappa) = \frac{1}{A(\kappa)} \oint_{A(\kappa)} \widehat{\phi}(X, \kappa) dA(\kappa) \tag{61}$$

where  $A(\kappa)$  is the spherical shell of radius  $\kappa$ , to obtain an equation that depends only on the scalar wave number and not anymore on the vector wave number implying a loss of directional information. The resulting equation reads

$$\begin{aligned} \frac{\partial \varphi_{ij}(X, \kappa, t)}{\partial t} + \langle u_k \rangle(X) \frac{\partial \varphi_{ij}(X, \kappa, t)}{\partial X_k} &= \mathcal{P}_{ij}(X, \kappa, t) + \mathcal{T}_{ij}(X, \kappa, t) \\ + \Psi_{ij}(X, \kappa, t) + \mathcal{J}_{ij}(X, \kappa, t) - \mathcal{E}_{ij}(X, \kappa, t) \end{aligned} \tag{62}$$

where the function  $\varphi_{ij}$  denotes the spherical mean of the Fourier transform of the two-point correlation tensor

$$\varphi_{ij}(X, \kappa, t) = (R_{ij}(X, \xi, t))^\Delta \tag{63}$$

This type of approach is the basis of spectral models developed in references [96, 97]. On the right and side of Eq. 62,  $\mathcal{P}_{ij}$  represents the production term defined by

$$\mathcal{P}_{ij}(X, \kappa, t) = -\varphi_{ik}(X, \kappa, t) \frac{\partial \langle u_j \rangle}{\partial X_k} - \varphi_{jk}(X, \kappa, t) \frac{\partial \langle u_i \rangle}{\partial X_k} \tag{64}$$

$\mathcal{T}_{ij}$  is the total transfer term defined by

$$\mathcal{T}_{ij}(X, \kappa, t) = \theta_{ij}(X, \kappa, t) + \zeta_{kimj}(X, \kappa, t) \frac{\partial \langle u_k \rangle}{\partial X_m} \tag{65}$$

where the first transfer term  $\theta_{ij}$  related to the triple velocity correlations is the inertial cascade

$$\theta_{ij}(X, \kappa, t) = - \left( \frac{\partial}{\partial \xi_k} (S_{i,kj} - S_{ik,j})(X, \xi, t) \right)^\Delta \tag{66}$$

whereas the second transfer term  $\zeta_{kimj}$  represents the fast transfer by action of mean velocity gradients

$$\zeta_{kimj}(X, \kappa, t) = - \left( \xi_m \frac{\partial R_{ij}}{\partial \xi_k}(X, \xi, t) \right)^\Delta \tag{67}$$

The redistribution term  $\Psi_{ij}$  takes the form as follows

$$\Psi_{ij}(\mathbf{X}, \kappa, t) = \frac{1}{\rho} \left( \frac{\partial \mathcal{K}_j}{\partial \xi_i} - \frac{\partial \mathcal{K}_i}{\partial \xi_j} \right) + \frac{1}{2\rho} \left( \frac{\partial \mathcal{K}_j}{\partial X_i} + \frac{\partial \mathcal{K}_i}{\partial X_j} \right) \tag{68}$$

where  $\mathcal{K}_i$  is the turbulent diffusion due to fluctuating pressure defined by

$$\mathcal{K}_i(\mathbf{X}, \kappa, t) = (K_{i(p)}(\mathbf{X}, \boldsymbol{\xi}, t))^\Delta = (K_{(p)i}(\mathbf{X}, \boldsymbol{\xi}, t))^\Delta \tag{69}$$

$\mathcal{J}_{ij}$  embodies all the diffusion like terms

$$\mathcal{J}_{ij}(\mathbf{X}, \kappa, t) = -\frac{1}{\rho} \left( \frac{\partial \mathcal{K}_j}{\partial X_i} + \frac{\partial \mathcal{K}_i}{\partial X_j} \right) - \frac{1}{2} \frac{\partial}{\partial X_k} (\varsigma_{i,kj} + \varsigma_{ik,j}) + \nu \frac{\partial^2 \varphi_{ij}(\mathbf{X}, \kappa)}{\partial X_l \partial X_l} \tag{70}$$

where the turbulent diffusion terms  $\varsigma_{i,jk}$  and  $\varsigma_{ik,j}$  are due to fluctuating velocities

$$\begin{aligned} \varsigma_{i,kj}(\mathbf{X}, \kappa, t) &= (S_{i,kj}(\mathbf{X}, \boldsymbol{\xi}, t))^\Delta \\ \varsigma_{ik,j}(\mathbf{X}, \kappa, t) &= (S_{ik,j}(\mathbf{X}, \boldsymbol{\xi}, t))^\Delta \end{aligned} \tag{71}$$

and the tensorial dissipation-rate  $\mathcal{E}_{ij}$  reads

$$\mathcal{E}_{ij}(\mathbf{X}, \kappa, t) = \frac{\nu}{2} \frac{\partial^2 \varphi_{ij}(\mathbf{X}, \kappa, t)}{\partial X_l \partial X_l} + 2\nu\kappa^2 \varphi_{ij}(\mathbf{X}, \kappa, t) \tag{72}$$

## 5.4 Integration in the spectral space

### 5.4.1 Single-scale turbulence models

The full integration of any variable  $\phi$  in the wave number ranges  $[0, \infty[$  of the spectral space is defined by

$$\phi(\mathbf{X}) = \int_0^\infty [\phi(\mathbf{X})]^\Delta(\kappa) d\kappa \tag{73}$$

The full integration of Eq. 62 allows to recover the usual statistical Reynolds stress model described by Eq. 20 where

$$R_{ij}(\mathbf{X}, t) = \int_0^\infty \varphi_{ij}(\mathbf{X}, \kappa) d\kappa \tag{74}$$

$$P_{ij}(\mathbf{X}, t) = \int_0^\infty \mathcal{P}_{ij}(\mathbf{X}, \kappa) d\kappa \tag{75}$$

$$\Pi_{ij}(\mathbf{X}, t) = \int_0^\infty \Psi_{ij}(\mathbf{X}, \kappa) d\kappa \tag{76}$$

$$\epsilon_{ij}(\mathbf{X}, t) = \int_0^\infty \mathcal{E}_{ij}(\mathbf{X}, \kappa) d\kappa \tag{77}$$

$$J_{ij}(\mathbf{X}, t) = \int_0^\infty \mathcal{J}_{ij}(\mathbf{X}, \kappa) d\kappa \tag{78}$$

Obviously, the integration of transfer term  $\mathcal{T}_{ij}$  vanished because the distance between the two points  $A$  and  $B$  goes to zero ( $\xi = 0$ ) in the physical space.

### 5.4.2 Multiple-scale turbulence models

The partial integration of Eq. 62 in the wave number ranges  $[\kappa_{m-1}, \kappa_m]$  of the spectral space allows to obtain the formulation of multiple-scale models [28, 98]. This one is not detailed here for the purpose of simplification.



### 5.4.3 Subgrid-scale turbulence models

The analysis is restricted to the case of homogeneous anisotropic turbulence for the sake of clarity and simplification. Consequently, the diffusion term vanishes. Subfilter scale stress models can be derived in a particular case where  $m = 2$  and by identifying the wave numbers  $\kappa_1 = \kappa_c$  and  $\kappa_2 = \kappa_d$ . Considering the wave number ranges such as  $[0, \kappa_c]$ ,  $[\kappa_c, \kappa_d]$  and  $[\kappa_d, \infty]$ , and by identifying the significant physical processes in each spectral zone, the integration of Eq. 62 leads to the three partial equations as follows

$$\frac{\partial R_{ij[0,\kappa_c]}}{\partial t} = P_{ij[0,\kappa_c]} - F_{ij}(\kappa_c) + \Pi_{ij[0,\kappa_c]} \tag{79}$$

$$\frac{\partial R_{ij[\kappa_c,\kappa_d]}}{\partial t} = P_{ij[\kappa_c,\kappa_d]} - F_{ij}(\kappa_d) + F_{ij}(\kappa_c) + \Pi_{ij[\kappa_c,\kappa_d]} \tag{80}$$

$$0 = F_{ij}(\kappa_d) - \epsilon_{ij[\kappa_d,\infty]} \tag{81}$$

where

$$R_{ij[0,\kappa_c]} = \int_0^{\kappa_c} \varphi_{ij}(\kappa, t) d\kappa \tag{82}$$

for the large resolved scales and

$$R_{ij[\kappa_c,\kappa_d]} = \int_{\kappa_c}^{\kappa_d} \varphi_{ij}(\kappa, t) d\kappa \tag{83}$$

for the small modeled scales. The fluxes of transfer of energy are computed by

$$F_{ij}(\kappa_c, t) = \mathcal{F}_{ij}(\kappa_c, t) - \varphi_{ij}(\kappa_c, t) \frac{\partial \kappa_c}{\partial t} \tag{84}$$

$$F_{ij}(\kappa_d, t) = \mathcal{F}_{ij}(\kappa_d, t) - \varphi_{ij}(\kappa_d, t) \frac{\partial \kappa_d}{\partial t} \tag{85}$$

with the definition

$$\mathcal{F}_{ij}(\kappa, t) = \int_{\kappa}^{\infty} \mathcal{T}_{ij}(\kappa', t) d\kappa' = - \int_0^{\kappa} \mathcal{T}_{ij}(\kappa', t) d\kappa' \tag{86}$$

The subgrid viscous dissipation-rate reads

$$(\epsilon_{ij})_{[\kappa_d,\infty[} = \int_{\kappa_d}^{\infty} \mathcal{E}_{ij}(\kappa, t) d\kappa \tag{87}$$

Equation 81 indicates that the tensorial dissipation-rate can be considered as a spectral flux that is independent of the cutoff wave number  $\kappa_c$ . Its theoretical expression is given by Eq. 87. Combining Eq. 80 with Eq. 81 gives the transport equation of the subgrid scale stress

$$\frac{\partial R_{ij[\kappa_c,\kappa_d]}}{\partial t} = P_{ij[\kappa_c,\kappa_d]} + F_{ij}(\kappa_c) + \Pi_{ij[\kappa_c,\kappa_d]} - (\epsilon_{ij})_{[\kappa_d,\infty[} \tag{88}$$

and in the contracted form, the transport equation of the subgrid-scale turbulent energy

$$\frac{\partial k_{[\kappa_c,\kappa_d]}}{\partial t} = P_{[\kappa_c,\kappa_d]} + F(\kappa_c) - \epsilon_{[\kappa_d,\infty[} \tag{89}$$

It is simple matter to show that  $R_{ij[\kappa_c,\kappa_d]}$  corresponds in fact to the statistical averaging of the subgrid scale fluctuating velocities  $\langle \tau(u_i, u_j) \rangle$ , more precisely

$$R_{ij[\kappa_c,\kappa_d]} = \langle \tau(u_i, u_j) \rangle = \langle (\tau_{ij})_{sgs} \rangle = \langle u_i^> u_j^> \rangle \tag{90}$$

Equation 88 looks like Eq. 52 although this one is written in a instantaneous form involving the stress  $(\tau_{ij})_{sgs}$  whereas Eq. 88 is written in a statistical sense involved the averaged sub-grid scale stress  $\langle(\tau_{ij})_{sgs}\rangle$ . As a consequence, we can assume that closures approximations used for statistical averaged equations also prevail in the case of large eddy simulations.

## 6 Hybrid RANS/LES Simulation

### 6.1 Principle of the method

Hybrid RANS/LES methods capable of reproducing a RANS-type behavior in the vicinity of a solid boundary and an LES-type behavior far away from the wall boundary have been developed in the past two decades for improving numerical prediction of complex flows encountered in engineering applications with affordable computational resources. In particular, depending on the physical problem to be studied, some regions of the flow may require a more refined description of the turbulent eddy interactions using finer grids with LES simulation whereas other regions that are of less complex physics can be calculated satisfactorily from RANS models [101–106]. As statistical and filtered equations can be written formally in the same mathematical form at a first sight, provided the commutation terms are negligible, (see Sections 3, 4 and 5), RANS and LES can be combined by using turbulence models based on different type of closure to build composite methods. The theoretical formalism developed in the spectral space in Section 5 also strengthens the idea that it is possible to unify the RANS and LES methodologies from a physical point of view in reconciling different physical descriptions. Usually, hybrid RANS/LES methods are inspired from RANS modeling that constitutes a convenient framework [92, 93]. According to the literature [49, 51], hybrid methods can be broadly classified into two main categories, zonal and non-zonal methods. RANS/LES zonal methods rely on two different models, a RANS model and a subgrid-scale model, which are applied in different domains separated by a sharp or dynamic interface whereas non-zonal methods assume that the governing set of equations is smoothly converting from a RANS behavior to an LES behavior, based on criteria updated during the computation. This terminology employed for classifying hybrid RANS-LES methods among zonal and non-zonal methods can be however ambiguous since both methods use different models in different regions. For this reason, some authors [14] prefer to identify on the one hand segregated modeling when different models RANS and LES based on a different structure of equations are used in each part of the computational domain, both RANS and LES computations are then performed in their respective domains separated by the interface and, on the other hand unified modeling corresponding to the counterpart to segregated modeling, considered as a more continuous approach, where here the RANS and LES models bear the same structure of equations. With segregated modeling, the flow solution including the velocity is discontinuous at the interface. Most of hybrid RANS-LES models were initially developed in the framework of a zonal approach [17–19], but more recently, new models based on a non-zonal approach [15, 26–28, 38–40, 46–48] are of growing interest in hybrid RANS-LES modeling for simulation of complex turbulent flows encountered in engineering applications.

### 6.2 Zonal models

Noticeably, the main shortcoming of these methods lies in the connection interface between the RANS and LES regions [102–104, 107–109]. The interface being empirically set inside

the computational domain, the turbulence closure changes from one model to another one without continuity when crossing the interface. An internal forcing produced by artificial instantaneous random fluctuations is then necessary for restoring continuity at the cross-flow between these domains in aiming to obtain correct velocity and stress profiles in the boundary layer. Extra terms introduced in the equations are then necessary to get the correct velocity and stress profiles in the boundary layer [110]. In particular, a thorough review on synthetic turbulence generators for RANS-LES interfaces in zonal simulations of aerodynamic problems was conducted recently by Shur et al. [111]. The question of the log-layer mismatch velocity for hybrid RANS/LES simulations has been addressed in detail by Hamba in Ref. [109]. Among these hybrid RANS/LES methods, the Detached Eddy Simulation (DES) developed by Spalart et al. [17–19], which was referred to as DES97 in its original version [20], where the model is switching from a RANS behavior to an LES behavior, depending on a criteria based on the turbulent length-scale, is one of the most popular method. However, although of practical use for aeronautical applications, DES is very sensitive to the grid-size. In particular, the gray area where the model varies from URANS to LES mode may be problematic unless the separation is abrupt and fixed by the geometry [20]. The second problem of DES is concerned with a possible delay in the formation of instabilities in mixing layers. Note that a new version of the detached-simulation, referred to as DDES [21], for delayed DES, resistant to ambiguous grid density, has been developed recently in this framework. Still from a practical point of view, the DES technique was afterwards applied on two-equation models such as for instance the  $k - \omega$  SST model [63] to convert it into the zonal  $k - \omega$  SST-DES model [23–25].

### 6.3 Non-zonal models

One of the first non-zonal hybrid RANS-LES method was derived by Speziale [15] hereafter denoted VLES98 for performing very large eddy simulation (VLES). In this method, the turbulent stresses are computed by damping the Reynolds stress stresses in regions where the grid spacing is of order of the Kolmogorov length-scale. This method presents the advantage to continuously vary between DNS and RANS computation and several VLES models were afterwards derived in this same line of thought. The partially integrated transport modeling (PITM) method is one of promising method in turbulence modeling developed by Schiestel and Dejoan [26], Chaouat and Schiestel [27, 31] because it allows numerical simulation of turbulent flows out of spectral equilibrium performed on relatively coarse grids. This one has become widespread in turbulence modeling because of its interest to dramatically reduce the computational resource in the field of engineering applications. The subfilter models derived in PITM have the property of working on LES mode and smoothly change from RANS to DNS if the grid-size is enough refined in the flow region with seamless coupling. The main ingredient of this method is the new dissipation-rate equation that is used in conjunction with the equation of the subfilter scale energy or equations of the subfilter scale stresses depending on the level of closure that is chosen. In particular, these authors have derived subfilter turbulence models, the former one using a two-equation subfilter energy model [26, 29] and the latter one, using a stress transport model based on second-moment closure [27, 30, 32]. The stress transport closure derived in the PITM framework was initially developed in the wave number space by Chaouat and Schiestel [27, 28], and its formalism afterwards was transposed to the frequency space by Fadai-Ghotbi et al. [112, 113] who obtained very similar equations. The partially averaged Navier-Stokes (PANS) method developed by Girimaji [39] also belongs to this line of thought, and the final equations have great similarities with the PITM equations. But the PANS equations were obtained on the

basis of practical arguments on turbulence. More precisely, the PANS method [37–41] has been formulated in the physical space by considering that the ratio for the subgrid energy to the total energy of turbulence, is arbitrary fixed in the flow without referring to the grid size of the mesh like in PITM. This assumption was used to derive turbulence models based on transport equations of the subgrid scale energy and dissipation-rate. The method of scale adaptive simulation (SAS) using two-equation models has been proposed by Menter and Egorov [46–48] to simulate unsteady turbulent flows. This method is based on the introduction of the Von Kármán length-scale into the turbulence scale equation. Like PANS, SAS must be however considered more as a URANS method than an hybrid RANS-LES method because no explicit filter or grid size appears in the formulation of its basic equations. Among non-zonal methods, one can notice also blending turbulence models using a weighted sum of a RANS model and LES model by means of blending factors such as for instance the one in Ref. [114] or the SBES model [115] that is promising.

#### 6.4 Zonal or non-zonal models?

The key issue to address now for the simulation of turbulent flow is whether one has to apply a zonal or a non-zonal model? This choice depends on several factors, mainly the type of the physical phenomena acting in the flow and the computer resources in terms of number of necessary grid-points and computational times that are available by the user. In the use of zonal modeling, the determination of the frontier between the zones must be motivated on physical phenomena involved in the flow field to be meaningful and how to manage the interface requires particular care. Non-zonal modeling presents the advantage to give a more consistent formalism. Some non-zonal models switch from RANS to LES using clipping parameters while others use a continuous formalism. The author considers that a non-zonal hybrid RANS/LES model that evolves continuously in LES mode between the two extreme limits of the spectrum that are RANS and DNS is more satisfactory from a physical point of view than a zonal model because it bridges two different levels of description in a consistent way. The model formulation may remain the same and does not pose some conceptual and numerical problems of an artificial separation between the RANS and LES regions. In such an hybrid RANS/LES simulation, the magnitude of the large scale fluctuating velocity  $u'$  is more or less large depending on the location of the cutoff wave number  $\kappa_c$  according to Eq. 28 and also on the physical processes involved in the flow such as interactions between the mean flow and turbulence. As it was mentioned, the question of the computer resource is of major importance in the choice of the model. In the case where the computer resources are large allowing a high grid resolution, the model can be simple in its formulation such as an eddy viscosity model assuming a direct constitutive relation between the turbulent stress and strain components only valid for fine grid turbulence. The resolved part of energy will be much larger than the modeled part of energy, and DES will be convenient. But conversely, when the memory resources are small leading to a poor grid resolution, the model should account for several transport equations of flow variables like PITM, PANS or SAS because the modeled part of energy can be appreciable in comparison with the resolved part of energy. Of course, in this case, it is not expected to get the accuracy of conventional fine grid simulation in the structural description of the flow, but some useful trends are however possible, the aim being to get acceptable results while hugely reducing the computational cost. Finally, it appears that these methods complement each other and are often implemented in combination.

## 7 Popular Hybrid RANS/LES Methods

There is a great variety of hybrid RANS/LES methods. The first hybrid methods have been historically introduced in the practical aim to tackle efficiently the problem of solving the wall region, which is by far the most usual type of real flow configuration in industrial and environmental practice. The RANS region near the wall was used as some convenient and economical boundary treatment. But this approach soon exhibited serious problems in the frontier between the two zones, may it be discontinuous or not. These problems depending on the type of models in use, they will be discussed in the following. Then the hybrid RANS/LES approach developed worldwide by several researchers undergo improvements and extended formalisms. Now continuous approaches are more and more preferred and applied to very different types of flows. The LES region and the RANS region of treatment are essentially determined by the local complexities of every particular flow or the type of description the user needs to obtain. Some degree of self adaptation can be active also. All these aspects are now discussed by considering the main usual methods of approach available at present time.

### 7.1 Very large eddy simulation (VLES)

The method was presented in its conceptual form VLES98 by Speziale in Ref. [15] and consists in evaluating the subgrid scale stresses  $(\tau_{ij})_{sgs}$  by means of a function  $F_R$  that controls the ratio of the part of modeled energy to resolved energy and the Reynolds averaged stresses  $R_{ij}$  as

$$(\tau_{ij})_{sgs} = F_R R_{ij} \quad (91)$$

The functions initially derived are of the form

$$F_R = [1 - \exp(-\beta \Delta / \eta_K)]^n \quad (92)$$

where  $\eta_K$  is the Kolmogorov length-scale,  $\beta$  and  $n$  are numerical parameters. In the limit where  $\Delta / \eta_K$  goes to zero, all relevant scales are resolved and the model behaves like DNS whereas when  $\Delta / \eta_K$  goes to infinity or is very large, the model goes to a RANS computation. But this function poses some problems when the Reynolds number is very large implying that the Kolmogorov length-scale  $\eta_K$  is very small. In this case, this function  $F_R$  goes to zero and the model gives a RANS behavior independently to the grid-size spacing, even for fine grids. Prior to every simulation, this method requires to perform a RANS computation to get an estimate of the Reynolds stresses  $R_{ij}$  as well as the Kolmogorov length-scale  $\eta_K$ . That said, the numerical values of the model parameters ( $\beta$  and  $n$ ) were not fixed in Ref. [15]. Fasel et al. [16] has applied this method to derive a VLES model based on the function given in Eq. 92 and two equation transport  $k - \epsilon$  model using the algebraic stress model (ASM) developed by Gatski and Speziale [58]. The numerical parameters used in this model were calibrated to  $\beta = 0.004$  and  $n = 1$ . These authors performed the wall jet flow that highlights the interaction between large structures developing in the free shear layer and the near wall boundary layer with encouraging results. This method was applied in its principle by Hsieh et al. [116] to derive a variant of VLES model using a generalized function  $F_R$  based on the turbulence energy spectrum  $E(\kappa)$  defined as

$$F_R = \frac{\int_{\kappa_c}^{\kappa_d} E(\kappa) d\kappa}{\int_{\kappa_e}^{\kappa_d} E(\kappa) d\kappa} \quad (93)$$

where  $\kappa_e$  and  $\kappa_d$  are the wave numbers corresponding to the integral length-scale of turbulence  $L_e = k^{3/2}/\epsilon$  and the Kolmogorov length-scale  $\eta_K$ , respectively. This model was applied to simulate the flow over an array of cubes placed in a plane channel. The hybrid RANS/LES simulation provided similar results as LES and better than unsteady RANS. Recently, Han and Krajnovic [117, 118] have built a new function  $F_R$  inspired both by Eqs. 92 and 93 as

$$F_R = \min \left[ 1, \left( \frac{1 - \exp(-\beta_1 \kappa_d / \kappa_c)}{1 - \exp(-\beta_2 \kappa_d / \kappa_e)} \right)^n \right] \tag{94}$$

where  $\beta_1 = 1.22 \times 10^{-3}$ ,  $\beta_2 = 2.0 \times 10^{-3}$  and  $n = 2$ . This model was used in conjunction with a turbulence model which takes the same form as the standard  $k - \epsilon$  model given by Eqs. 13 and 14 using the Boussinesq viscosity assumption defined in Eq. 45 but the turbulent eddy viscosity was modified as  $\nu_{sgs} = F_R \nu_t$  where  $\nu_t$  is given by Eq. 12. The motivation of this model was to provide a proper LES mode between the RANS and DNS limits. In practice, it was found that the VLES model behaves like a RANS model in the near-wall region within the viscous sublayer and like a VLES mode in other regions that approaches LES in the limit of fine mesh resolution. This model was applied to simulate the periodic hill flow at the Reynolds number  $Re = 10595$ , as well as turbulent flows past a square cylinder at  $Re = 22000$  and a circular cylinder at  $Re = 3900$  and  $140000$ . Then, Han and Krajnovic [119] have developed a VLES model based on the  $k - \omega$  model [62] including the function  $F_R$  given by Eq. 94 to better describe the near wall turbulence where the turbulent eddy viscosity is then given by  $\nu_t = F_R k / \omega$ . They performed numerical simulations of the turbulent flow past a circular cylinder at  $Re = 3900$  and  $Re = 3 \times 10^6$  and obtained satisfactory results on coarse meshes.

## 7.2 Detached eddy simulation (DES)

### 7.2.1 S-A DES model

The detached eddy simulation (DES) developed by Spalart and co-authors in its original version DES97 [17–19] including its variant delayed version DES (DDES) [21] and the improved delayed detached eddy simulation (IDDES) [22] is one of the most popular method used for the simulation of high Reynolds number flows with massive separation around obstacles, with the aim to access global coefficients such as the drag, lift and pressure coefficients that are useful in the aerodynamic design optimization of aircraft wings. In this approach, the model is switching from a RANS mode in the boundary layer to LES mode in the core flow, depending on a criterion based on the turbulence length-scale. This approach is zonal but considering that the same basic model is used both in the RANS and LES zones, the transition between the two zones occurred in the so-called “gray-zone” is made without true discontinuity. The success and weakness of the DES method were mentioned by Spalart in Ref. [20]. These DES models are based on the Spalart-Allmaras RANS model [59, 60] described by Eq. 11 where the wall distance  $d_w$  is replaced by  $\tilde{d}$  involving the grid-size  $\Delta$

$$\tilde{d} = \min(d_w, C_{DES} \Delta) \tag{95}$$

where

$$\Delta = \max(\Delta_1, \Delta_2, \Delta_3) \tag{96}$$

$C_{DES}$  is a coefficient set to 0.65 which has been calibrated in the decaying homogeneous turbulence. In the near wall region,  $\Delta_1 \approx \Delta_2 \gg \Delta_3$ , so that  $\Delta = \Delta_1$  and  $\tilde{d} = d_w$ , the model reduces to the S-A model whereas far away from the wall,  $d_w \gg \Delta$  leading to  $\tilde{d} = C_{DES} \Delta$

and the model acts as a subgrid scale model. The gray zone corresponds to the interface region where  $d_w \approx C_{DES}\Delta$ . In this version of the model, the separation of the boundary layer is controlled by the RANS model. This model was used to simulate aerodynamic flow such as for instance a mixing layer and the flow over a backward-facing step [17], the flow past a circular cylinder including laminar or turbulent separation at the Reynolds numbers  $Re = 5 \times 10^4$ ,  $1.4 \times 10^5$  and  $3 \times 10^6$  [18], and the flow with massive separation around the aircraft F-15E at  $65^\circ$  angle of attack at the Reynolds number  $Re = 13.6 \times 10^6$  and Mach number 0.3 [120]. Spalart and al. [21] have pointed out that the original DES model can exhibit an incorrect behavior in thick boundary layers when the grid spacing parallel to the wall becomes less than the boundary layer thickness  $\delta$ . In this case, DES unsuccessfully attempts LES, as the eddy viscosity is lower than that from the RANS S-A model, but the resolved Reynolds stresses have not developed. The delayed DES model has been then proposed with a RANS mode in thick boundary layers without preventing LES mode after massive separation. To overcome this shortcoming, the DES length-scale was redefined as follows [21]

$$\tilde{d} = d_w - f_d \max(0, d_w - C_{DES}\Delta) \tag{97}$$

where  $f_d$  is a shielding function which takes on the value unity in the LES region and reduces to zero elsewhere. The authors have proposed the hyperbolic function  $f_d = 1 - \tanh([8r_d]^3)$  where the dimensionless parameter  $r_d$  corresponds to the ratio (squared) of the length-scale involved in the mean shear rate to the distance from the wall,  $r_d = (v + v_t)/(\sqrt{S}C_K^2 d_w^2)$ , where  $\tilde{S} = \partial\bar{u}_i/\partial x_j \partial\bar{u}_i/\partial x_j$ . This model was applied to various flow configurations such as the backward facing step, circular cylinder, single and multi-element airfoil [21]. As an illustrative example, Spalart et al. used this DDES model to simulate the flow around a rudimentary landing gear characterized itself by the separation of the turbulent boundary layer [121]. The standard DDES model was improved by Shur et al. [22] by combining the DDES with a wall modeling in LES (WMLES), mainly to resolve the mismatch between the inner modeled log layer and the outer resolved log-layer produced by the RANS and LES mode, respectively. Overall, the IDDES model was empirically built in order to perform external flows with massive separation like DES or DDES and improves DDES in case of mixed flow with both attached and separated regions. To do that, the authors have modified the computation of the length-scale given by Eq. 97 firstly by introducing a blending functions  $\tilde{f}_d$  such as

$$\tilde{d} = \tilde{f}_d(1 + f_e)d_w + (1 - \tilde{f}_d)C_{DES}\Psi\Delta \tag{98}$$

where  $\tilde{f}_d$ ,  $f_e$  and  $\Psi$  are empirical functions and secondly by modifying the estimate of the grid spacing  $\Delta$  as indicated in Ref. [22]. This model was evaluated in the case of a plane channel and a plane hydrofoil with trailing edge separation [22] and applied by several authors for performing different types of flows such as for instance the flow around a pair of cylinders in tandem [122, 123], the NACA 5510 airfoil flow [124]. In a different spirit, a purely zonal DES model (ZDES) in which RANS and DES domains are selected individually was proposed by Deck [125, 126]. As pointed out by Spalart [20], ZDES is less self-sufficient than DES and there is the concern that for complex flow subjected to a smooth-wall separation, the DES mode is normally not known at the time the zone are set. Referring to Section 6.4, it seems that this latter zonal approach raises more questions than it answers and should be discarded for the simulation of too complex turbulent flows. Improvement of DES based on S-A model is still an active field of research [127]. Note at least that the logarithmic-layer mismatch (LLM) of the mean velocity in DES simulation

resulting from the grid size effects near the wall has been investigated by several authors [20, 83, 84] and in particular by Nikitin et al. [128] giving a clear diagnosis on this problem.

### 7.2.2 DES based on two-equation models

The principle of the DES method has been initially applied to the S-A Spalart Allmaras model but it was then generalized to any RANS model in order to derive its corresponding DES-RANS model.

The basic idea relies on Eq. 95 where in this case, the turbulence length-scale is computed as

$$L_{DES} = \min(L_{RANS}, C_{DES}\Delta) \tag{99}$$

where  $L_{RANS}$  denotes the length-scale computed by the RANS mode. The basic two-equation  $k - \epsilon$  model defined by Eqs. 13 and 14 is transformed into the  $k - \epsilon$  DES model by modifying the dissipation term in the kinetic energy equation as

$$\frac{\partial k_{sgs}}{\partial t} + \frac{\partial}{\partial x_j} (k_{sgs} \bar{u}_j) = P_{sgs} - F_{DES} \epsilon_{sgs} + (J_k)_{sgs} \tag{100}$$

$$\frac{\partial \epsilon_{sgs}}{\partial t} + \frac{\partial}{\partial x_j} (\epsilon_{sgs} \bar{u}_j) = c_{\epsilon 1} \frac{\epsilon_{sgs}}{k_{sgs}} P_{sgs} - c_{\epsilon 2} \frac{\epsilon_{sgs}^2}{k_{sgs}} + (J_\epsilon)_{sgs} \tag{101}$$

where

$$F_{DES} = \max\left(1, \frac{k_{sgs}^{3/2}/\epsilon_{sgs}}{C_{DES}\Delta}\right) \tag{102}$$

It is of interest to study the extreme limits of this model. In the case where  $k_{sgs}^{3/2}/\epsilon_{sgs} > C_{DES} \Delta$ , one gets  $F_{DES} \epsilon_{sgs} = k_{sgs}^{3/2}/C_{DES} \Delta$ , the model behaves like the one equation LES model given by Eqs. 48 and 50 whereas in the contrary case where  $k_{sgs}^{3/2}/\epsilon_{sgs} < C_{DES} \Delta$ , one gets  $F_{DES} \epsilon_{sgs} = \epsilon_{sgs}$  and the model behaves like the usual RANS  $k - \epsilon$  model given by Eqs. 13 and 14. If we will see that this method returns good results in the following, Eq. 100 poses some problems from a physical point of view because the dissipation-rate is modified by the function  $F_{DES}$  although in principle, it should not be affected by the cutoff wave number  $\partial \epsilon_{sgs} / \partial \kappa_c = 0$ . Indeed, it must be interpreted as a flux of energy that is transferred from the large scales to the small scales. This is demonstrated in Section 5 by Eq. 81 leading to the resulting equation 89. In the framework of DES using two-equation models, Strelets [23], Travin et al. [24] then proposed a zonal  $k - \omega$  SST-DES model based on the RANS model [63]. These authors performed a large variety of flows such as the NACA 0012 airfoil beyond stall, flows around circular cylinder as well as separated flow in the backward-facing step. As a result, this model did not show any clear superiority over the S-A-DES model. Menter et al. [25] have presented the full formulation of a zonal  $k - \omega$  SST-DES model inspired from the SST model [63] accounting for a variant of the function  $F_{DES}$  leading to the  $k - \omega$  SST-DDES model. These equations formally read

$$\frac{\partial k_{sgs}}{\partial t} + \frac{\partial}{\partial x_j} (k_{sgs} \bar{u}_j) = P_{sgs} - F_{DES} \beta^* \omega_{sgs} k_{sgs} + (J'_k)_{sgs} \tag{103}$$

$$\frac{\partial \omega_{sgs}}{\partial t} + \frac{\partial}{\partial x_j} (\omega_{sgs} \bar{u}_j) = \alpha \nu_t P_{sgs} - \beta \omega_{sgs}^2 + (J_\omega)_{sgs} + (C_{k\omega})_{sgs} \tag{104}$$

where  $P_{sgs}$  denotes the production term,  $(J'_k)_{sgs}$  and  $(J_\omega)$  are the diffusion terms. The function  $F_{DES}$  is still inspired from Eq. 102 but the coefficient  $C_{DES}$  is computed by means of a blending function  $F_1$  corresponding to the two branches of the SST model



$C_{DES} = (1 - F_1)C_{DES}^{k-\omega} + F_1C_{DES}^{k-\omega}$  as defined in Ref. [24]. In Ref. [25], the function  $F_{DES}$  is computed using a variant version as

$$F_{DES} = \max \left( 1, \frac{k_{sgs}^{3/2}/\epsilon_{sgs}}{C_{DES}\Delta} (1 - F_{SST}) \right) \tag{105}$$

where  $F_{SST}$  is a function selected from the blending functions of the SST model [63]. This function  $F_{DES}$  has the effect to reduce the influence of the DES limiter on the boundary layer portion of the flow. The quantity  $(C_{k\omega})_{sgs}$  is a cross-term involving the gradients  $\partial k_{sgs}/\partial x_j$  and  $\partial \omega_{sgs}/\partial x_j$ ,  $\alpha$  and  $\beta$  are computed from a blending operation from the corresponding constants of  $k - \epsilon$  and the  $k - \omega$  models. These terms appearing in Eqs. 103 and 104 are given in detail in Ref. [25]. Note however that the notations have been changed here to clearly make the difference between mean statistical variables used in RANS and subgrid-scale variables used in LES. This model was applied to simulate the flow around a cube mounted inside a 2D channel and it returned good results [25]. One can also mention for instance the simulation of plane impinging jets with the  $k - \omega$  DES model [130]. As for DES based on S-A model, DDES and IDDES based on the  $k - \omega$  SST model, to date, constitute a part in the work of hybrid RANS-LES modeling that is actively pursued by several authors [131]. For illustration purposes of the IDDES method, several applications are briefly presented in the following. Figure 2 describes the flow around tandem cylinders representative of a simplified landing gear accounting for  $11 \times 10^6$  cells where the spanwise dimension is given by  $L_3/D = 3$ . This visualization displays the capability of the simulation to resolve fine-grained turbulence and exhibits the vortical structures [122, 123].

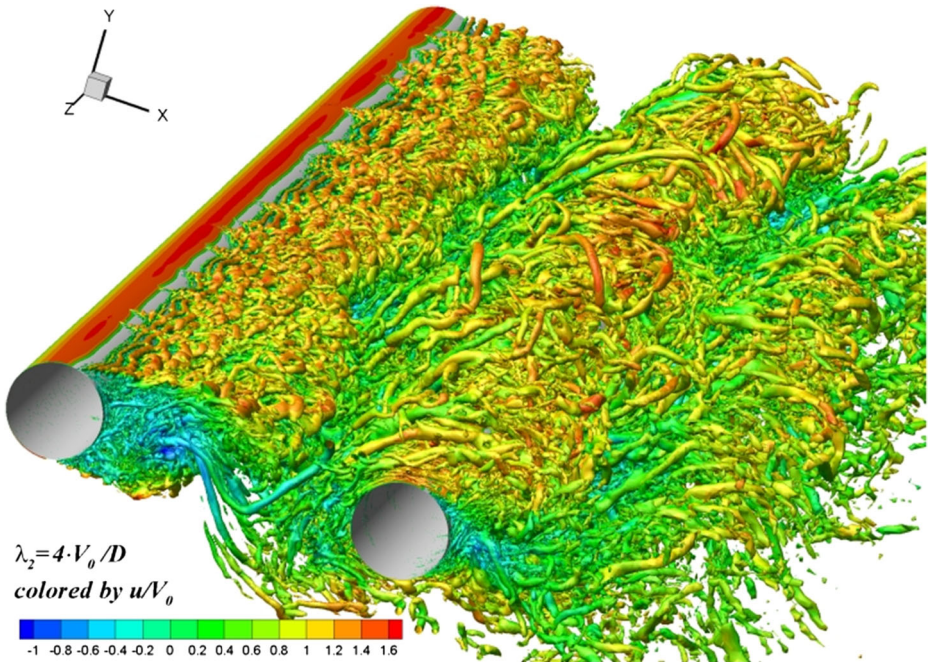


**Fig. 2** IDDES simulation of the flow around around tandem cylinders at the Reynolds number  $Re_D = V_o D/\nu = 1.66 \times 10^5$  [122, 123]. Isosurfaces of swirl colored by the streamwise velocity ( $\lambda = 4V_o/D$ ). Grid of  $11 \times 10^6$  cells. (Courtesy of P.R. Spalart (Boeing, USA) and M. Strelets (NTS, Russia))

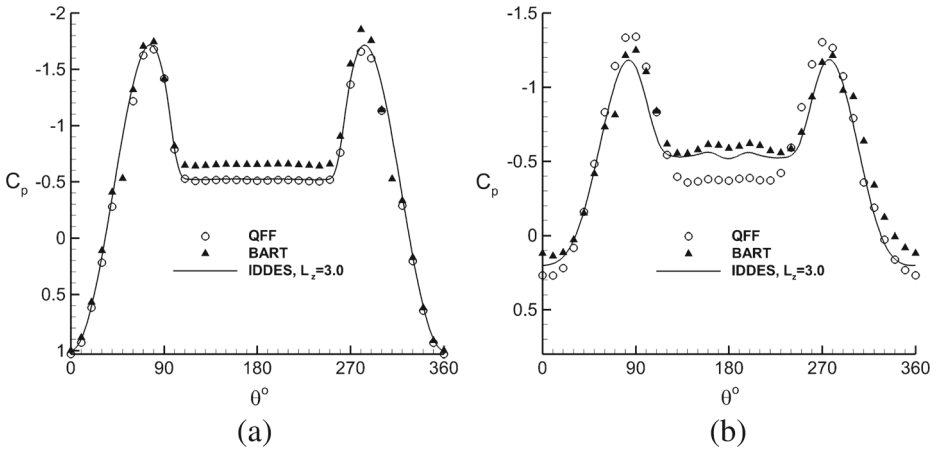


**Fig. 3** IDDES simulation of the flow around tandem cylinders at the Reynolds number  $Re_D = V_o D/\nu = 1.66 \times 10^5$  [122, 123]. Surface pressure distributions over the upstream (a) and downstream (b) cylinders. (Courtesy of P.R. Spalart (Boeing, USA) and M. Strelets (NTS, Russia))

Overall, the prediction of this turbulent flow including the pressure coefficient on both cylinders, power spectral densities as well as velocity and turbulent energy profiles were found in relatively good agreement with the experiment [122, 123]. Figure 3 displays the surface pressure distributions over the upstream (a) and downstream (b) cylinders returned by the IDDES simulation in comparison with the measurements from wind tunnels (BART and QFF) at NASA LaRC. The next application is concerned with space launchers. Figure 4

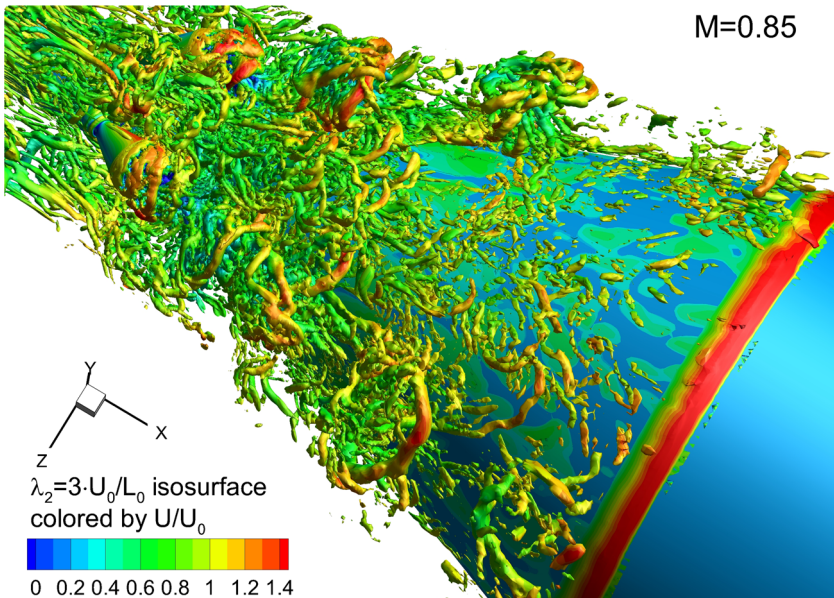


**Fig. 4** IDDES simulation of the flow around a nozzle of a launch escape system at the Mach number  $M = 0.85$ . Isosurfaces of swirl colored by the streamwise velocity ( $\lambda = 3V_o/D$ ). Grid of  $25 \times 10^6$  cells. (Courtesy of Garbaruk et al. [129])

shows the flow structures around a nozzle of a launch escape system at the Mach number  $M = 0.85$ . This simulation has been performed on a fine grid of  $25 \times 10^6$  cells and provided the determination of the mean flow and evaluation of integral forces [129].

### 7.3 Partially integrated transport modeling (PITM) method

#### 7.3.1 Basic equations

Generally speaking, the PITM method based on the spectral (62) allows to convert any RANS model to its corresponding subfilter scale model. In regards with conventional LES [70], the PITM method enables to simulate turbulent flows on relatively coarse grids when the cutoff wave number can be placed before the inertial zone as far as the grid-size is however sufficient to describe correctly the mean flow. The PITM method is founded on the technique of partial spectral integration introduced in Refs. [26–28]. In this presentation, the case of homogeneous anisotropic turbulence is considered for sake of clarity and simplification so that the diffusion terms vanish and the variable  $X$  appearing in Eq. 62 is omitted. As a result, Eq. 88 involving the transport equation of the subfilter-scale stress  $(\tau_{ij})_{sfs}$  can be rewritten in a more compact form as

$$\frac{\partial \langle (\tau_{ij})_{sfs} \rangle}{\partial t} = \langle (P_{ij})_{sfs} \rangle + \langle (\Pi_{ij})_{sfs} \rangle - \langle (\epsilon_{ij})_{sfs} \rangle \tag{106}$$

where

$$\langle (P_{ij})_{sfs} \rangle = (P_{ij})_{[\kappa_c, \kappa_d]} + F_{ij}(\kappa_c) \tag{107}$$

$$\langle (\Pi_{ij})_{sfs} \rangle = (\Pi_{ij})_{[\kappa_c, \kappa_d]} \tag{108}$$

$$\langle (\epsilon_{ij})_{sfs} \rangle = (\epsilon_{ij})_{[\kappa_d, \infty[} \tag{109}$$

and in a contracted form

$$\frac{\partial \langle k_{sfs} \rangle}{\partial t} = \langle P_{sfs} \rangle - \langle \epsilon_{sfs} \rangle \tag{110}$$

where  $k_{sfs}$  is the subfilter scale turbulent energy. So, at the wavenumber  $\kappa_d$ , all the preceding hypotheses imply  $F(\kappa_d) = \epsilon \approx \langle \epsilon_{sfs} \rangle$ , the turbulence Reynolds number being supposed to be large. Like in the RANS multiscale approach [98], the variable wavenumber  $\kappa_d$  is defined such that

$$\kappa_d - \kappa_c = \zeta \frac{\langle \epsilon_{sfs} \rangle}{\langle k_{sfs} \rangle^{3/2}} \tag{111}$$

where the value of the numerical coefficient  $\zeta$  is chosen such that the wavenumber  $\kappa_d$  is always sufficiently large in order to leave the entire inertial region before it and also that the spectral energy beyond  $\kappa_d$  is negligible. This practice allows to avoid infinite integration bounds and within these hypotheses it is a fair approximation to suppose that the energy flux through the splitting at wavenumber  $\kappa_d$  is equal to the dissipation rate. Moreover, the relation (111) together with the choice of the coefficient  $\zeta$  provides a dynamical mean for continuously adjusting the location of the cutoff wavenumber just after the inertial zone while the spectrum is still evolving. So, the difference in the wave numbers  $(\kappa_d - \kappa_c)$  stays nicely in scale in the spectrum. The dissipation rate equation is then obtained by taking the

derivative of Eq. 111 with respect to time using Eqs. 84 and 85 written in a contracted form and also taking into account Eq. 110. One can then easily obtain [26–28]

$$\frac{\partial \langle \epsilon_{sfs} \rangle}{\partial t} = c_{sfs\epsilon_1} \frac{\langle \epsilon_{sfs} \rangle}{\langle k_{sfs} \rangle} \langle P_{sfs} \rangle - c_{sfs\epsilon_2} \frac{\langle \epsilon_{sfs} \rangle^2}{\langle k_{sfs} \rangle} \tag{112}$$

where

$$c_{sfs\epsilon_1} = \frac{3}{2} \tag{113}$$

and as a main result, it is found that

$$c_{sfs\epsilon_2} = \frac{3}{2} - \frac{\langle k_{sfs} \rangle}{(\kappa_d - \kappa_c) E(\kappa_d)} \left[ \left( \frac{\mathcal{F}(\kappa_d) - F(\kappa_d)}{\epsilon} \right) - \frac{E(\kappa_d)}{E(\kappa_c)} \left( \frac{\mathcal{F}(\kappa_c) - F(\kappa_c)}{\epsilon} \right) \right] \tag{114}$$

Setting  $\kappa_d \gg \kappa_c$ , and  $E(\kappa_d) \ll E(\kappa_c)$ , Eq. 114 reduces to

$$c_{sfs\epsilon_2} = \frac{3}{2} - \frac{\langle k_{sfs} \rangle}{\kappa_d E(\kappa_d)} \left( \frac{\mathcal{F}(\kappa_d) - F(\kappa_d)}{\epsilon} \right) \tag{115}$$

Taking then the corresponding equation for  $\kappa_c = 0$  in a pure RANS modeling,

$$c_{\epsilon_2} = \frac{3}{2} - \frac{k}{\kappa_d E(\kappa_d)} \left( \frac{\mathcal{F}(\kappa_d) - F(\kappa_d)}{\epsilon} \right) \tag{116}$$

and combining these Eqs. 115 and 116 as explained in Refs. [26, 27], it is then simple matter to show that

$$c_{\epsilon_{sfs2}} = \frac{3}{2} + \frac{\langle k_{sfs} \rangle}{k} \left( c_{\epsilon_2} - \frac{3}{2} \right) \tag{117}$$

As it is demonstrated in detail in Ref. [32], the numerical value  $c_{\epsilon_{sfs1}} = 3/2$  can be re-adjusted to a different value and the more general expression for  $c_{\epsilon_{sfs2}}$  is

$$c_{\epsilon_{sfs2}} = c_{\epsilon_1} + \frac{\langle k_{sfs} \rangle}{k} (c_{\epsilon_2} - c_{\epsilon_1}) \tag{118}$$

The ratio  $\langle k_{sfs} \rangle/k$  appearing in Eq. 117 can be calibrated as a function of the location of the cutoff wave number. In the first version of the PITM models [26, 27], this ratio was computed by integrating the Kolmogorov law in the wave number range  $[\kappa_c, \infty[$ . The resulting expression was then empirically modified to satisfy the limit when  $k_{sfs}$  approaches  $k$  leading to

$$c_{\epsilon_{sfs2}} = c_{\epsilon_1} + \frac{c_{\epsilon_2} - c_{\epsilon_1}}{1 + \beta \eta_c^{2/3}} \tag{119}$$

where  $\eta_c = \kappa_c L_e$  and  $\beta = 2/(3C_K)$ . This dimensionless parameter  $\eta = \kappa L_e$  is interpreted as a dimensionless wavenumber with the turbulence length-scale  $L_e = k^{3/2}/\epsilon$ . Then, in more advanced PITM models, the universal spectrum [30]

$$E(\kappa) = \frac{\frac{2}{3}\beta(\kappa L_e)^{\alpha-1} L_e k}{[1 + \beta(\kappa L_e)^\alpha]^\gamma} \tag{120}$$

where  $\alpha$  and  $\beta$  are constant coefficients given by  $\alpha\gamma = 2/3$  and  $\beta = [2/(3C_K)]^\gamma$  to comply with the Kolmogorov law, was considered to better describe the spectrum at the origine of small wave numbers. Indeed, in this region, the spectrum behaves like  $E(\kappa) = \propto \kappa^{\alpha-1}$  taking into account the hypothesis of permanence of very large eddies. Using Eq. 120, it is a simple matter to compute the ratio  $k_{sfs}/k$ , leading to the more accurate computation of the coefficient  $c_{\epsilon_{sfs2}}$  than Eq. 119 as

$$c_{\epsilon_{sfs2}} = c_{\epsilon_1} + \frac{c_{\epsilon_2} - c_{\epsilon_1}}{[1 + \beta \eta_c^\alpha]^\gamma} \tag{121}$$

In practice [30–36], the coefficients used in Eq. 120 are  $\alpha = 3$  and  $\gamma = 2/9$ . The function given by Eq. 121 introduced in the subfilter-scale model equation allows to sensitize the model to the grid-size  $\Delta$  or in a more general way, the filter width that may be larger than the grid-size [33]. The coefficient  $c_{\epsilon_{sfs2}}$  can be considered as a dynamical parameter which draws the spectral distribution towards the prescribed equilibrium distribution given by Eq. 120. In other words, this term acts like a relaxation towards the Kolmogorov equilibrium spectrum. In PITM like in LES methodology, the turbulence model is formulated using the framework of filtering of equations.

### 7.3.2 Subfilter scale eddy viscosity models

The filtered transport equation of the subfilter scale energy corresponding to Eq. 110 reads

$$\frac{Dk_{sfs}}{Dt} = P_{sfs} - \epsilon_{sfs} + J_{sfs} \tag{122}$$

where  $D/Dt$  denotes the material derivative defined by  $D/Dt = \partial/\partial t + \bar{u}_k \partial/\partial x_k$ . The production term  $P_{sfs}$  due to the interaction between the subfilter stress and the filtered velocity gradient is given by Eq. 49. The turbulent stresses  $(\tau_{ij})_{sfs}$  are proportional to the filtered deformation of the flow field according to Eq. 45 where the eddy viscosity is defined by

$$\nu_{sfs} = c_\mu \frac{k_{sfs}^2}{\epsilon_{sfs}} \tag{123}$$

The diffusion term  $J_{sfs}$  appearing in Eq. 122 is modeled by a gradient law hypothesis according to Eq. 51. The filtered transport equation of the subfilter dissipation-rate corresponding to Eq. 112 reads

$$\frac{D\epsilon_{sfs}}{Dt} = c_{sfs\epsilon_1} \frac{\epsilon_{sfs}}{k_{sfs}} P_{sfs} - c_{sfs\epsilon_2} \frac{\epsilon_{sfs}^2}{k_{sfs}} + (J_\epsilon)_{sfs} \tag{124}$$

The coefficient  $c_{sfs\epsilon_1} = c_{\epsilon_1}$  whereas  $c_{sfs\epsilon_2}$  is given by Eq. 121. The diffusion term  $(J_\epsilon)_{sfs}$  embedded in Eq. 124 for handling non-homogeneous flows is modeled using a gradient law hypothesis

$$(J_\epsilon)_{sfs} = \frac{\partial}{\partial x_j} \left[ \left( \nu + \frac{\nu_{sfs}}{\sigma_\epsilon} \right) \frac{\partial \epsilon_{sfs}}{\partial x_j} \right] \tag{125}$$

where  $\sigma_\epsilon$  is a constant coefficient.

### 7.3.3 Subfilter scale stress models

The filtered transport equation of the subfilter scale stress corresponding to Eq. 106 reads

$$\frac{D(\tau_{ij})_{sfs}}{Dt} = (P_{ij})_{sfs} + (\Pi_{ij})_{sfs} - (\epsilon_{ij})_{sfs} + (J_{ij})_{sfs} \tag{126}$$

where the terms appearing in the right-hand side of this equation are identified as subfilter production, redistribution, dissipation and diffusion, respectively. The production term  $(P_{ij})_{sfs}$  accounts for the interaction between the subfilter stresses and the filtered velocity gradients is given by Eq. 53. The redistribution term  $(\Pi_{ij})_{sfs}$  appearing in Eq. 126 is modeled assuming that the interaction mechanisms of the subgrid scales with the resolved scales of the turbulence is of the same nature than the interaction mechanisms involving all the fluctuating scales with the main flow. So that Eqs. 22 and 23 established in RANS modeling can be transposed to LES. Taking into account this argument, the redistribution

term  $(\Pi_{ij})_{sfs}$  is also decomposed into a slow part  $(\Pi_{ij}^1)_{sfs}$  that characterizes the return to isotropy due to the action of subgrid turbulence on itself

$$\left(\Pi_{ij}^1\right)_{sfs} = -c_{1sfs} \frac{\epsilon_{sfs}}{k_{sfs}} \left( (\tau_{ij})_{sfs} - \frac{1}{3} (\tau_{mm})_{sfs} \delta_{ij} \right) \tag{127}$$

and a rapid part,  $(\Pi_{ij}^2)_{sfs}$  that describes the action of the filtered velocity gradients

$$\left(\Pi_{ij}^2\right)_{sfs} = -c_2 \left( (P_{ij})_{sfs} - \frac{1}{3} (P_{mm})_{sfs} \delta_{ij} \right) \tag{128}$$

where  $c_{1sfs}$  plays the same role as the Rotta coefficient  $c_1$  but is no longer constant whereas  $c_2$  is the same coefficient used in RANS modeling. In practice, the function  $c_{1sfs}$  is modeled as  $c_{1sfs} = c_1 \alpha(\eta)$  where  $\alpha$  is an increasing function of the parameter  $\eta$  to strengthen the return to isotropy for large wave numbers. The diffusion terms  $(J_{ij})_{sfs}$  is modeled assuming a well-known gradient law

$$(J_{ij})_{sfs} = \frac{\partial}{\partial x_m} \left( v \frac{\partial (\tau_{ij})_{sfs}}{\partial x_m} + c_s \frac{k_{sfs}}{\epsilon_{sfs}} (\tau_{ml})_{sfs} \frac{\partial (\tau_{ij})_{sfs}}{\partial x_l} \right) \tag{129}$$

where  $c_s$  is a constant coefficient. The subfilter tensorial transfer rate  $(\epsilon_{ij})_{sfs}$  approached by  $2/3 \epsilon_{sfs} \delta_{ij}$  at high Reynolds number is computed by its transport (124) but the diffusion term  $(J_\epsilon)_{sfs}$  is then modeled by a gradient tensorial law

$$(J_\epsilon)_{sfs} = \frac{\partial}{\partial x_j} \left( v \frac{\partial \epsilon_{sfs}}{\partial x_j} + c_\epsilon \frac{k_{sfs}}{\epsilon_{sfs}} (\tau_{jm})_{sfs} \frac{\partial \epsilon_{sfs}}{\partial x_m} \right) \tag{130}$$

where  $c_\epsilon$  is a constant coefficient. The subfilter model is extended to low Reynolds number turbulence in Ref. [35].

### 7.3.4 Limiting behavior for the subfilter model

From a theoretical point of view, it is of interest to analyze the asymptotic behavior of the subfilter stress model when the cutoff location approaches the upper limit of the energy spectrum wavenumber interval. Considering a spectral equilibrium situation in the inertial zone governed by the Kolmogorov law, the theoretical ratio of the subfilter energy to the total energy reaches the value

$$\frac{\langle k_{sfs} \rangle}{k} \approx \frac{3C_K}{2} \eta_c^{-2/3} \tag{131}$$

In this case, it is a straightforward matter to show that the subfilter characteristic length scale goes to the filter width

$$\frac{\langle k_{sfs} \rangle^{3/2}}{\langle \epsilon_{sfs} \rangle} = \frac{\Delta}{\pi} \left( \frac{3C_K}{2} \right)^{3/2} \tag{132}$$

The subfilter scale stress model allows to compute the stress  $(\tau_{ij})_{sfs}$  thanks to the transport (126) and (124) so that the concept of the turbulent viscosity is discarded. But it is still possible to define a tensorial viscosity given by  $(v_{ij})_{sfs} = c_\mu \langle k_{sfs} \rangle (\tau_{ij})_{sfs} / \epsilon_{sfs}$ . For the sake of clarity, due to the fact that the small scales become isotropic at high Reynolds number,  $\lim_{\eta_c \rightarrow \infty} \langle (\tau_{ij})_{sfs} \rangle = 2/3 \langle k_{sfs} \rangle \delta_{ij}$ , it is simpler to analyze the case of a scalar viscosity given by  $\nu_{sfs} = c_\mu \langle k_{sfs} \rangle^2 / \langle \epsilon_{sfs} \rangle$ . Assuming a local equilibrium situation inside a very small slice in the far end of the energy spectrum,  $\langle \epsilon_{sfs} \rangle = 2\nu_{sfs} \langle \bar{S}_{ij} \bar{S}_{ij} \rangle$ , it can be

shown for a two-equation model [30] that the limiting behavior for the subfilter viscosity  $\nu_{sfs}$  is then given by

$$\nu_{sfs} = \frac{1}{\pi^2} \left( \frac{3C_K}{2} \right)^3 c_\mu^{3/2} \Delta^2 \sqrt{2 \langle \tilde{s}_{ij} \tilde{s}_{ij} \rangle} \quad (133)$$

This expression shows that the subfilter model behaves like the Smagorinsky model given by Eq. 46 where the Smagorinsky constant  $C_s$  can be easily identified.

### 7.3.5 Applications

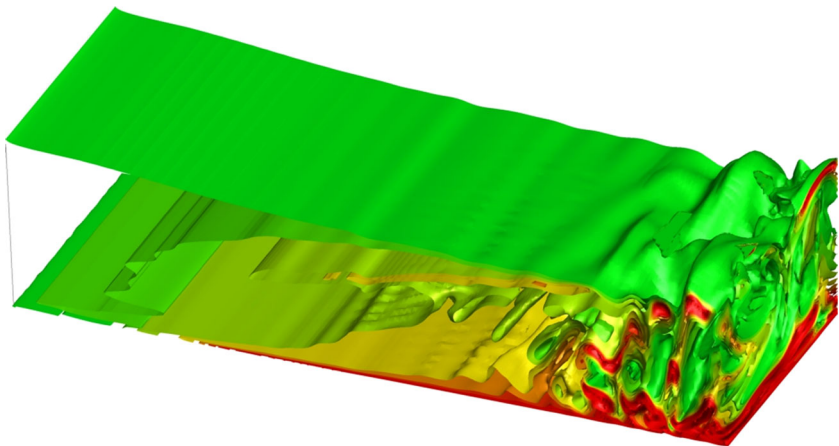
The PITM models were first validated against the fully turbulent channel flow [26, 27] and the decaying isotropic turbulence in/out of spectral equilibrium [26, 30]. This latter test case was relevant to verify that the PITM method preserves the concept of the energy cascading process independently of any spectral cutoff location [26]. Previous simulations have also shown that the PITM method was able to reproduce fairly well a large variety of internal and external flows. The subfilter scale eddy viscosity model accounting for Eqs. 122, 124, 123 was used to simulate turbulent pulsed flows [26] and a mixing of two turbulent flows of differing scales [29], but also with an additional equation for the temperature variance, thermal convection at high Rayleigh numbers [132], whereas the subfilter scale stress models accounting for Eqs. 126 and 124 was applied to perform rotating flows encountered in turbomachinery at the bulk Reynolds number  $R_b = U_b \delta / \nu = 14000$  and at different rotation numbers  $R_o = \Omega \delta / U_b$  varying from moderate, medium and very high rotation rates  $R_o = 0.17, 0.50$  and  $1.50$  [31], flows in a plane channel with appreciable fluid injection through a permeable wall which corresponds to the propellant burning in solid rocket motors [27], flows over periodic hills with separation and reattachment of the boundary layer both at the Reynolds number  $Re = 10595$  [34, 133, 134] and  $Re = 37000$  [35], airfoil flows at the Reynolds number  $Re = 1.64 \times 10^6$  for an angle of attack  $12^\circ$  [135], a turbulent flow in a small axisymmetric contraction at the bulk Reynolds number  $R_b = 4.47 \times 10^5$  [36]. Overall, it is found that the subfilter scale model behaves like a RANS model in the wall region and like LES in the core flow. Moreover, the part of the modeled energy can be appreciable in comparison with the resolved part of energy. For instance, the modeled energy represents roughly 50% of energy even in the center of the channel far away from the walls for the simulation of the flow in a small axisymmetric contraction while providing fair results [36]. These PITM simulations allowed a drastic reduction of the required computational resources in comparison with those necessary for performing highly resolved LES. This point will be discussed through elements of comparison of several models in Table 2. For illustration purposes of the PITM method, different types of turbulent flows are presented in the following.

Figure 5 displays the isosurfaces of the instantaneous spanwise filtered vorticity  $\bar{\omega}_i = \epsilon_{ijk} \partial \bar{u}_k / \partial x_j$  in the channel flow with fluid injection through the lower wall while the upper wall is impermeable [27]. This figure reveals the detail of the flow structures as well as the location of the transition process from the laminar to turbulent flow regime. One can observe that the vortical structures appear two-dimensional in the upstream transition location and break down to form three-dimensional structures after the flow transition. In the downstream transition location, the flow is then characterized by the presence of roll-up vortex structures of large magnitude of vorticity in the spanwise direction as also reproduced in highly resolved LES [136]. This simulation performed on coarse grids returned the mean velocity, turbulent stresses and transition location in good agreement with the experiment

**Table 2** Simulations of turbulent flows performed on fine and coarse grids, respectively

| Engineering applications  | Authors                    | Turbulence model | Grid points                        |
|---------------------------|----------------------------|------------------|------------------------------------|
| Mixing of turbulent flows | Wengle et al. [141]        | DSM              | $4.0 \times 10^6$                  |
|                           | Befeno and Schiestel [29]  | PITM             | $3.6 \times 10^5$                  |
| Flows with wall injection | Apte and Yang [136]        | DSM              | $9.0 \times 10^6$                  |
|                           | Chaouat and Schiestel [27] | PITM             | $1.4 \times 10^6$                  |
| Flows in rotating frame   | Lamballais et al. [138]    | SFM              | $8.0 \times 10^5$                  |
|                           | Chaouat [31]               | PITM             | $7.4 \times 10^4, 8.8 \times 10^5$ |
| Flows over periodic hills | Fröhlich et al. [142]      | DSM/WALE         | $4.6 \times 10^6$                  |
|                           | Breuer et al. [143]        | DSM              | $13.1 \times 10^6$                 |
| $Re = 10595$              | Saric et al. [144]         | DES              | $4.8 \times 10^5, 1.0 \times 10^6$ |
|                           | Saric et al. [145]         | DDES             | $2.4 \times 10^5$                  |
|                           | Friess et al. [134]        | equiv-DES        | $9.6 \times 10^5$                  |
|                           | Menter and Egorov [47]     | SST-SAS          | $2.5 \times 10^6$                  |
|                           | Ma et al. [146]            | PANS             | $4.1 \times 10^5$                  |
|                           | Chaouat [34]               | PITM             | $2.4 \times 10^5$                  |
| $Re = 37000$              | Manhart et al. [147]       | SM,WALE,LAG      | $1.0 \times 10^6, 3.8 \times 10^6$ |
|                           | Ma et al. [146]            | PANS             | $1.5 \times 10^6$                  |
|                           | Chaouat and Schiestel [35] | PITM             | $4.8 \times 10^5, 9.6 \times 10^5$ |

[137]. Figure 6 describes the isosurfaces of the instantaneous vorticity modulus in the channel flow subjected to a spanwise rotation where the rotation rate  $R_o = 1.50$  is here very high [31]. A first glimpse of sight reveals that the PITM simulation provides some dynamical elements of the flow in wall turbulence by the presence of very large-scale longitudinal roll cells in the anticyclonic wall region and clearly illustrates the three-dimensional nature of



**Fig. 5** PITM simulation of a turbulent flow in a plane channel with fluid injection through the lower surface [27]. Isosurfaces of instantaneous filtered vorticity  $\bar{\omega}_i = \epsilon_{ijk} \partial \bar{u}_k / \partial x_j$  in the streamwise direction. The flow undergoes a transition process from laminar to turbulent regime. The bulk Reynolds number  $R_b = U_b \delta / \nu$  varies from 0 at the head end of the channel to  $10^5$  at the exit section. Grid of  $400 \times 44 \times 80 \approx 1.4 \times 10^6$  points



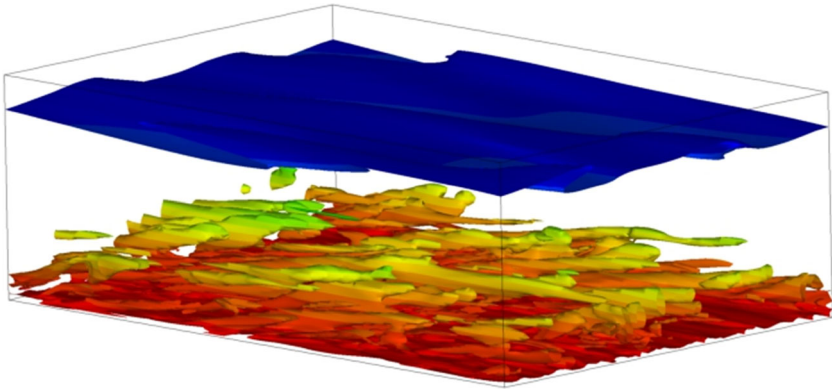


**Fig. 6** PITM simulation of a rotating channel flow [31]. Isosurfaces of vorticity modulus  $\omega = 3u_m/\delta = 12 \cdot 10^5$ . Colored according to the pressure contours. Anticyclonic wall region: down; Cyclonic wall region: up.  $R_m = 14000$ ,  $R_o = 1.50$ . Grid of  $124 \times 84 \times 84 \approx 0.9 \times 10^6$  points

the flow although the geometry is two-dimensional. In comparison with non-rotating flows, the vorticity roll cells appear less inclined with respect to the wall,  $10^\circ - 15^\circ$  instead of  $45^\circ$  [138]. Figure 7 shows the  $Q$  isosurfaces [139] of the turbulent flows over periodic hills at the high Reynolds number  $R_b = U_b\delta/\nu = 37000$  [35] and reveals also the presence of very large longitudinal roll cells that develop in the entire channel. Due to the flow recirculation, a strong turbulence activity is visible near the lower wall and particularly concentrated in the leeward region of the second hill. Obviously, RANS or even URANS models cannot reproduce these instantaneous roll cell structures because of the long-time averaging process. Considering that the gross structural features are satisfactorily approached, they are a favorable indication for energy level predictions. Overall, the velocity and the turbulence

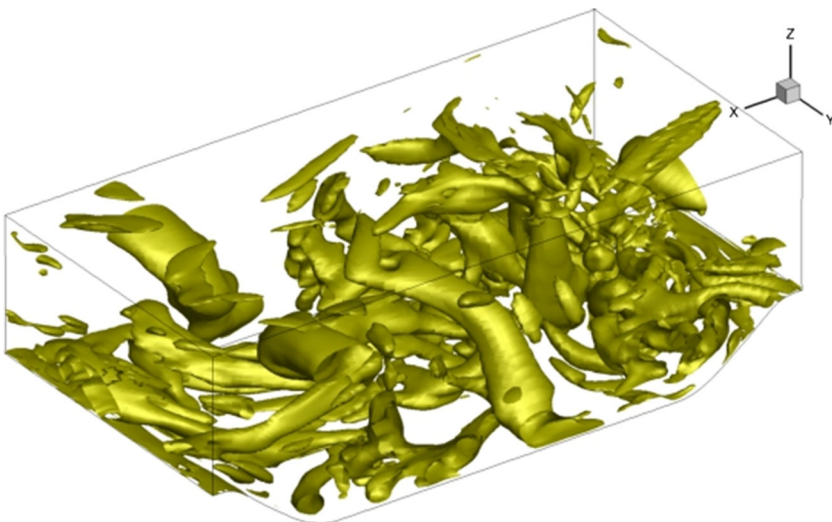


**Fig. 7** PITM simulation of the turbulent flow over periodic hills at  $Re = 37000$  [35]. Vortical activity illustrated by the  $Q$  isosurfaces,  $Q = 4 \cdot 10^5 s^{-2}$ . Grid of  $160 \times 60 \times 100 \approx 10^6$  points

stresses were found in good agreement with the experiment [140]. This is shown in Fig. 8 that exhibits the mean streamwise velocity  $\langle u_1 \rangle / U_b$  as well as the turbulent shear stress  $\tau_{13} / U_b^2$  at two cross stations  $x_1/h = 2$  and 6. The selected positions encompass the regions in the middle of the recirculation zone close to the leeward hill face  $x_1/h \approx 2$ , prior to the reattachment  $x_1/h = 4$  and the flow recovery  $x_1/h = 6$ . At the position  $x_1/h = 2$ , the velocity near the wall is negative showing that the boundary layer is detached (except for the RANS-RSM calculation). The maximum reverse flow occurs in this region. But at the position  $x_1/h = 6$ , the boundary layer is again attached. The PITM simulation returns mean velocity profiles that exhibit a very good agreement with the reference data, but on the other hand, the RANS computation exhibits inaccurate results. The total shear stresses  $\tau_{ij}$  includes the subfilter and resolved parts of energy. One can see that the PITM shear

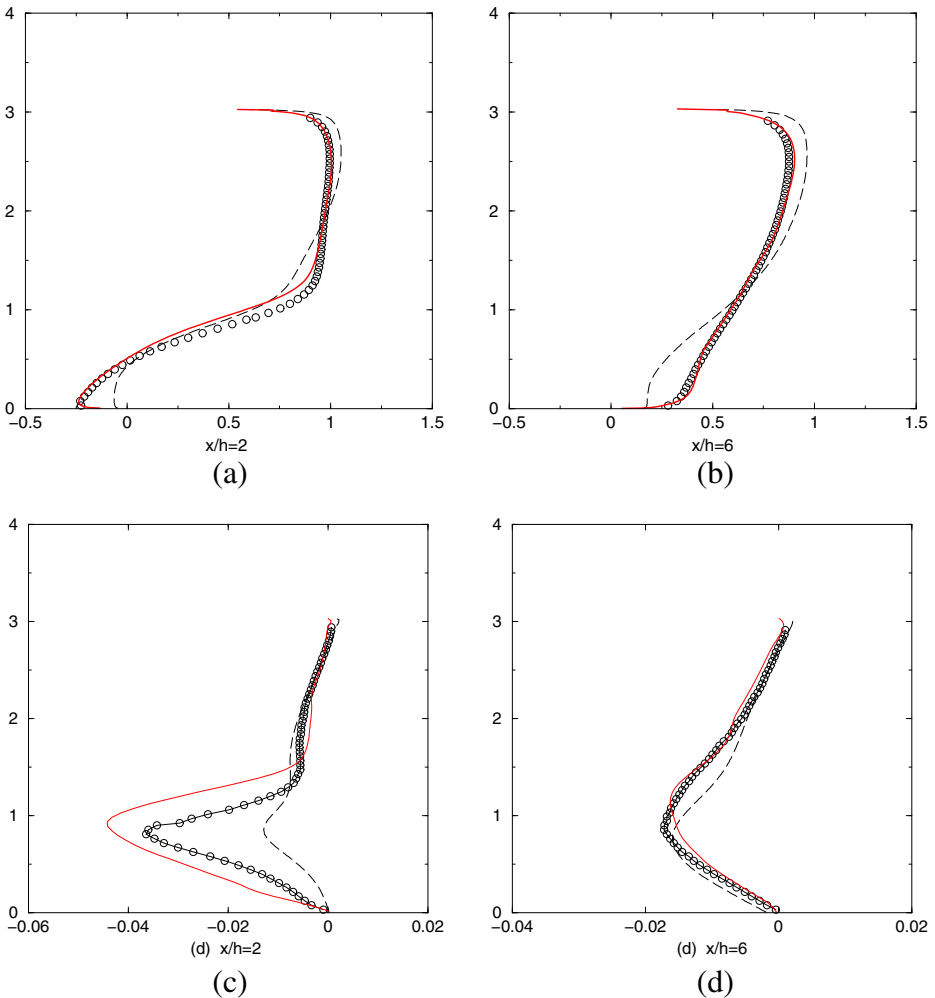


**Fig. 8** Flow over periodic hills at  $Re = 37000$  [35]. Mean streamwise velocity  $\langle u_1 \rangle / U_b$  (a),(b) and turbulent shear stress  $\tau_{13} / U_b^2$  (c),(d) at different locations ( $x_1/h = 2$  and 6). PITM ( $160 \times 60 \times 100$ ) —; RSM computation —( $80 \times 30 \times 100$ ). Experiment  $\circ$  [140]

stress profiles present a quantitative good agreement with the reference data even if some slight differences are visible. As for the mean velocity, the RSM stresses highly deviate from the reference data in the two positions of the channel. Finally, as the question of CPU time requirement is of first importance in numerical simulation, note that the additional cost resulting from the solving of the PITM subfilter scale stress model including seven transport equations requires only roughly 30 % to 50 % more CPU time than eddy viscosity models, so that the benefit to apply an advanced turbulence modeling is greatly appreciated. Table 2 summarizes the characteristics of several LES and hybrid RANS/LES simulations for comparison purpose.

### 7.3.6 Temporal partially integrated transport modeling method

Although the PITM formalism is built in the spectral space of wave numbers considering the concept of the tangent homogeneous space at a point of non-homogeneous flow field [28], it is of interest to note that this method was recently transposed to the space of frequencies assuming inhomogeneous stationary flows by Fadai-Ghotbi et al. [112, 113] leading to the temporal PITM (TPITM) method. These authors have considered temporal filters instead of physical space filters to handle non-homogeneous stationary flows. The TPITM method was also used to derive the dissipation-rate equation in an analogous manner as in standard PITM. As an important result, they showed that the dissipation-rate equation finally takes exactly the same formulation as the one found in the spectral space by the original PITM method. In particular, Eq. 118 was recovered confirming its general character. These authors then developed a subfilter-scale stress model [113] using the elliptic blending method [148] and proposed a dynamic procedure to better drive the model toward the expected amount of modeled/resolved energy that can be interpreted as a return to equilibrium process [32].

## 7.4 Partially averaged Navier-Stokes (PANS) method

### 7.4.1 Basic equations

The partially averaged Navier-Stokes (PANS) method developed by Girimaji [37, 39, 40] is based on the self-similarity scale assumption in the physical space. In spite of a totally different background developed independently from PITM, the basic PANS transport equations look similar in their general form to the PITM equations. However, in the PANS method, the ratio of the subfilter-energy to the total energy  $f_k = k_{sgs}/k$  and the ratio  $f_\epsilon = \epsilon_{sgs}/\epsilon$  are arbitrarily and empirically prescribed to fixed values for each computation, whereas in the PITM method, they are dynamically computed in time and space in connection with the filter width. The PANS solution is then depending on these prescribed ratios, implying that the filter becomes disconnected from the method. The role of the filter involved in the cutoff wave number of the energy spectrum cannot anymore be clearly interpreted from a physical point of view. Indeed, the PITM method provides a physical foundation in spectral space that allows to make a clear link between the unresolved-to-total ratios and the filter length scale whereas the PANS in the contrary does not address this question. Because of this argument, the PANS method is however questionable in principle for tackling all applications and especially for simulating non-equilibrium flows with departures from the standard Kolmogorov law involving transfer of energy between the small scales and large scales. This point was discussed in detail in Ref. [32]. Consequently, although of practical interest for CFD, this method poses some problems in its overall consistency. For simplicity, the PANS method is presented here in the case of homogeneous turbulence. The extension to the case

of non-homogeneous turbulence is made by embedding the diffusion terms in the equations as discussed earlier. Considering that  $f_k$  is constant, it is simple matter to get

$$\frac{\partial k_{sgs}}{\partial t} = P_{sgs} - \epsilon_{sgs} = f_k \frac{\partial k}{\partial t} = f_k (P - \epsilon) \tag{134}$$

leading to

$$P = \frac{P_{sgs} - \epsilon_{sgs}}{f_k} + \frac{\epsilon_{sgs}}{f_\epsilon} \tag{135}$$

Assuming also that  $f_\epsilon$  is constant leads to

$$\frac{\partial \epsilon_{sgs}}{\partial t} = f_\epsilon \frac{\partial \epsilon}{\partial t} = f_\epsilon \left[ c_{\epsilon_1} \frac{P\epsilon}{k} - c_{\epsilon_2} \frac{\epsilon^2}{k} \right] = c_{\epsilon_1} P f_k \frac{\epsilon_{sgs}}{k_{sgs}} - c_{\epsilon_2} \frac{f_k}{f_\epsilon} \frac{\epsilon_{sgs}^2}{k_{sgs}} \tag{136}$$

By substituting Eq. 135 into Eq. 136, it is simple matter to obtain the resulting equation

$$\frac{\partial \epsilon_{sgs}}{\partial t} = c_{\epsilon_1} \frac{P_{sgs}\epsilon_{sgs}}{k_{sgs}} - c_{sgs\epsilon_2} \frac{\epsilon_{sgs}^2}{k_{sgs}} \tag{137}$$

where

$$c_{sgs\epsilon_2} = c_{\epsilon_1} + \frac{f_k}{f_\epsilon} (c_{\epsilon_2} - c_{\epsilon_1}) \tag{138}$$

In practice, PANS simulations are performed with the function  $f_\epsilon$  set to unity [37, 39, 40]. The original PANS method was developed assuming that  $f_k$  takes on a constant value [37] and extensive applications have been worked out in this framework [39, 40]. The PANS method was extended to the case where  $f_k$  is a function in space given itself by a preliminary RANS computation [41, 43] according to the proposal of Girimaji and Abdol-Hamid [38] as follows

$$f_k \geq \frac{1}{\sqrt{c_\mu}} \frac{\Delta}{L_e} \tag{139}$$

to require that the grid-size is larger than the smallest resolved length scale. This variant PANS version denoted here VPANS to clearly mention that the simulation is performed with a constant RANS  $f_k$ -field in space given by Eq. 139 throughout the whole computation was applied to simulate the test case of an axisymmetric jet at different grid resolutions [38]. A new formulation of the function  $f_k$  has been used afterwards [45] based on partial integration of the complete Von Kármán energy spectrum  $E(\kappa)$  as introduced earlier in PITM [26, 30] leading to a new extended PANS formalism hereafter denoted EXPANS to avoid confusion with PANS. In the PANS model, the diffusion terms can be embedded in the equations for simulating non-homogeneous flows [39, 40]. Several authors have then improved the basic eddy viscosity model derived from the PANS method. Basara et al. [43] have developed a four-equation PANS model inspired from the RANS  $k - \epsilon - \zeta - f$  model where  $\zeta = (\tau_{22})_{sgs}/k_{sgs}$  and  $f$  is a parameter related to the pressure-strain correlation term accounting for the elliptic relaxation model [148] whereas Ma et al. [146] have proposed a low Reynolds number PANS formulation using damping functions for approxaching walls.

### 7.4.2 Applications

The PANS model has been used for simulating complex flows encountered in engineering applications such as the turbulent flows past a square and circular cylinder [42, 149], the flow around a rudimentary landing gear [44], the flows over periodic hills both at the Reynolds number  $Re = 10595$  and  $Re = 37000$  [146], the flow around a simplified vehicle model [150, 151] as well bluff body flows [152]. These applications often emphasize the ability of the approach to simulate big unsteady eddying motions.

## 7.5 Scale adaptive simulation (SAS)

### 7.5.1 Basic equations

The method of scale adaptive simulation (SAS) has been proposed by Menter and Egorov [46, 47] to simulate unsteady turbulent flows by using two-equation models. This method is based on the introduction of the generalized Von Kármán length-scale  $L_{vK}$  defined as

$$L_{vK} = K \sqrt{\frac{2\langle S_{ij} \rangle \langle S_{ij} \rangle}{\frac{\partial^2 \langle u_i \rangle}{\partial x_k^2} \frac{\partial^2 \langle u_j \rangle}{\partial x_l^2}}} \tag{140}$$

given by the Rotta’ equation [66] into the turbulence scale equation,  $K$  being the von Kármán constant. The meaning of this turbulence length-scale is simple. For a boundary layer, the Von Kármán length-scale  $L_{vK}$  is the distance normal to the wall  $x_n$  in the logarithmic layer region assuming that the velocity gradient is given by  $\partial \langle u_1 \rangle / \partial x_n = u_\tau / K x_n$  where  $u_\tau$  is the friction velocity. Menter and Egorov [46, 47] indicated in their paper that the accounting for the von Kármán length-scale into RANS models allows the corresponding SAS models to dynamically adjust to resolved structures in a URANS simulation, which results in a LES-like behavior in unsteady regions of the flow field while acting like standard RANS models in stable flow regions. This argument is supported by the test case of turbulent shear flow. In the case of homogeneous shear flow, the frequency  $\omega$  is proportional to the mean strain rate while the length-scale  $L$  goes to infinity. In the case of non-homogeneous flows, the frequency is proportional to the local strain rate but the spatial variation of length-scale  $L$  is then limited by  $L_{vK}$ . For unsteady flows, the model has the feature to work in a SAS mode because the turbulence length-scale is reduced yielding a lower eddy viscosity that allows the development of turbulent fluctuations. More details of the principle of the SAS method can be found in Refs [46, 47]. The SAS method relies on local flow physics rather than the grid-size to make the transition from RANS to LES-like behavior. In that sense, the SAS method has been derived entirely from the RANS formalism given in Section 3.2 without referring to the filter or the grid-size  $\Delta$  (or equivalently the cutoff wave number  $\kappa_c$ ). So that this one must be considered more as an unsteady RANS method than a hybrid RANS-LES method. This point is of importance because contrarily to VLES, DES and PITM methods, SAS does not revert to DNS in the limiting condition where the grid-size  $\Delta$  goes to the Kolmogorov length-scale  $\eta_K$ . Initially, Menter and Egorov [46, 47] have derived the transport equation for the variable  $\Psi = kL$  inspired from the work of Rotta [66] and they have then introduced the variable  $\Phi = \sqrt{k}L$  by a simple transformation of variables since this one is directly proportional to the turbulent eddy viscosity  $\nu_t = c_\mu^{1/4} \Phi$ . As a result, they proposed the K-square-root K-L (KSKL) model that formally reads

$$\frac{\partial k}{\partial t} + \frac{\partial}{\partial x_j} (k \langle u_j \rangle) = P - c_\mu^{3/4} \frac{k^2}{\Phi} + J_k \tag{141}$$

and

$$\frac{\partial \Phi}{\partial t} + \frac{\partial}{\partial x_j} (\Phi \langle u_j \rangle) = \frac{\Phi}{k} P \left( \zeta_1 - \zeta_2 \left( \frac{L}{L_{vK}} \right)^2 \right) - \zeta_3 k + J_\Phi \tag{142}$$

where  $J_\Phi$  denotes the diffusion process associated with  $\Phi$ ,  $\zeta_1$ ,  $\zeta_2$  and  $\zeta_3$  being numerical coefficients. This model was tested on the case of the flow around a cylinder at the

Reynolds number based on the diameter  $Re = 3.6 \times 10^6$  [47] as well as the well known decaying isotropic turbulence. In comparison with the  $k - \omega$  SST model which returns only large scale fluctuations, it has been found that the KSKL model allowed the formation of turbulent structures, in the separated zone past the cylinder due to the vortex shedding instability. Afterwards, the KSKL model was transformed into the  $k - \omega$  SAS model using the relation

$$\Phi = \frac{1}{c_\mu^{1/4}} \frac{k}{\omega} \tag{143}$$

To do that, the additional term involving the ratio of the length-scale  $(L/L_{\nu K})^2$  appearing in Eq. 142 was included as a source term in the  $\omega$  equation of the  $k - \omega$  SST model to convert it into the  $k - \omega$  SST-SAS model. This source term usually retained reads [46, 47]

$$Q_{SAS} = \max \left[ \zeta_2 S^2 \left( \frac{L}{L_{\nu K}} \right)^2 - C_{SAS} \frac{2k}{\sigma_\Phi} \max \left( \frac{1}{k^2} \frac{\partial k}{\partial x_j} \frac{\partial k}{\partial x_j}, \frac{1}{\omega^2} \frac{\partial \omega}{\partial x_j} \frac{\partial \omega}{\partial x_j} \right), 0 \right] \tag{144}$$

where  $C_{SAS} = 2$ ,  $\sigma_\Phi = \sigma_k$  used in the diffusion term of  $J_k$  and the length-scale  $L$  is then given by  $L = \sqrt{k} / (C_\mu^{1/4} \omega)$ . This term  $Q_{SAS}$  dominates the other terms appearing in the  $\omega$  equation in situation of unsteady flows implying an increase of  $\omega$  leading to a decrease of the turbulent eddy viscosity since  $\nu_t = k/\omega$ . At last, note that SAS provides a continuous variation of solution ranging from LES-type to RANS type with respect to the time step  $\Delta t$  corresponding to the CFL number selected in the simulation.

### 7.5.2 Applications

The SAS method was applied to simulate the flow over periodic hills at the Reynolds number  $Re = 10595$  on a coarse grid using different CFL [47]. The SAS simulations returned mean velocity profiles in good agreement with reference LES for each CFL. Other cases such as the backward facing step flow and the flow around a triangular cylinder were simulated [47]. The  $k - \omega$  SST-SAS model was finally used to simulate a large variety of turbulent flows encountered in practical engineering applications as detailed in Ref. [48]. Recent elements and application of SAS to complex flows in industrial CFD can be found in Ref. [153]. With the aim to illustrate the potential of SAS and its basic difference with standard URANS models, several turbulent flows are presented in the following. Figure 9 shows the  $Q$  isosurfaces [139] of the turbulent flow around a circular cylinder at the Reynolds number  $Re = 3.6 \times 10^6$  simulated with both the SST-URANS and KSKL models using the same grid and the same time step (CFL). Contrarily to what happens for the SST-URANS simulation that produces only organized roll cell structures, it can be seen that the KSKL simulation reproduces the vortex shedding instability that is put in light by the formation of turbulent structures past the cylinder. The next Fig. 10 is concerned with an airfoil flow with massive flow separation at low Mach number. The angle of attack is  $\alpha = 60^\circ$  and the Reynolds number takes on the value  $Re = 2.7 \times 10^5$ . The simulation has been performed using the SST-SAS model with a time scale equal to 3% of the convective time scale corresponding to a CFL of about unity. This figure shows the  $Q$  isosurfaces [139] of the flow illustrating the turbulent structures behind the airfoil. As a result, this simulation predicted

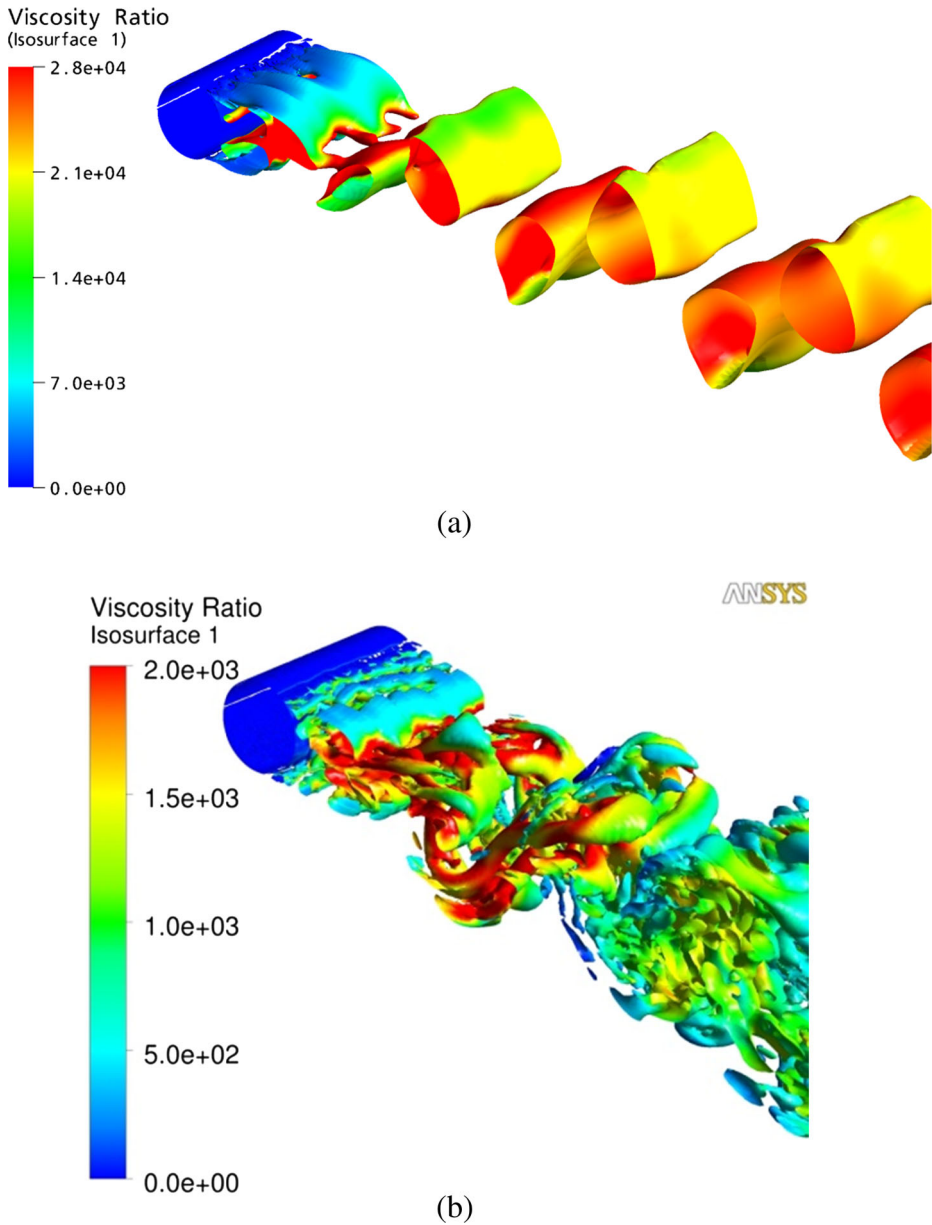


**Fig. 9** Simulation of the turbulent flow around a circular cylinder in a cross flow at  $Re = 3.6 \times 10^6$  [47]. **a** SST-URANS **(b)** KSKL model.  $Q$  Isosurfaces colored according to the eddy viscosity ratio  $\mu_t/\mu$ , smaller by factor 14 in **(b)** (Courtesy of Menter and Egorov [47].)

fairly well the lift and drag coefficients with 2% accuracy compared to the measurements [48]. More precisely, Fig. 11 shows the evolution of the mean pressure coefficient returned by the SST-SAS simulation. A good agreement is observed with the experimental data.

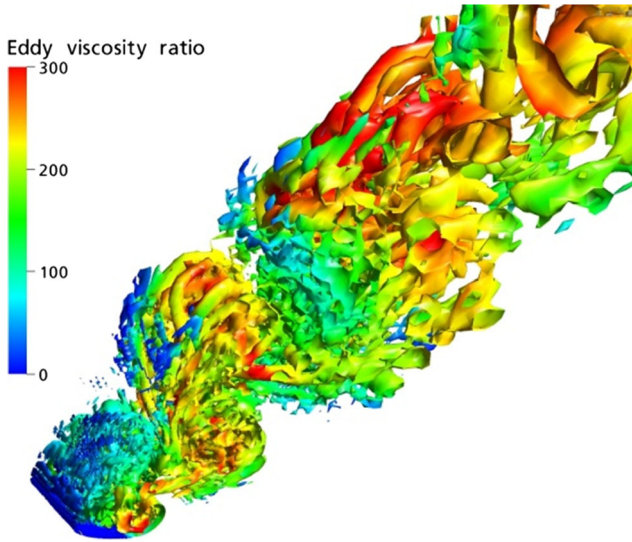


**Fig. 10** SST-SAS simulation of the turbulent flow around the NACA0021 airfoil [48]. Turbulent structures.  $Q$  isosurfaces colored according to the eddy viscosity ratio  $\mu_t/\mu$ .  $\alpha = 60^\circ$ ,  $Re = 2.7 \times 10^5$ . Grid of  $140 \times 101 \times 134 \approx 1.9 \times 10^6$  points. (Courtesy of Egorov et al. [48])

## 8 Link Between some Hybrid RANS/LES Methods

### 8.1 PITM and PANS methods

Although the PITM method has been developed in the spectral space on the basis of the physical processes of transfer of energy into the spectral zone of the spectrum whereas the PANS method has been empirically developed in the physical space involving a self similarity evolution hypothesis, the PANS method has made an important step towards PITM when Foroutan and Yavuzkurt [45] introduced the technique of partial integration of a Von Karman spectrum as previously developed in PITM, in the new extended PANS

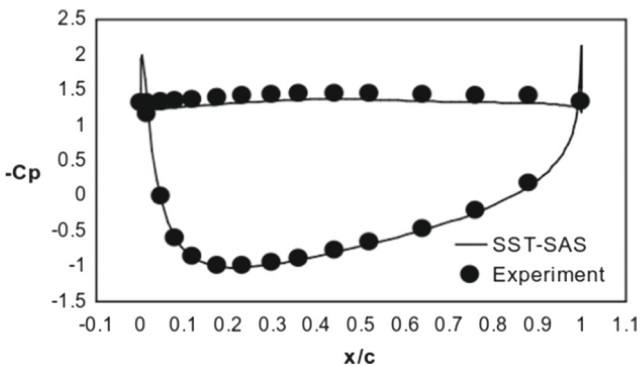


**Fig. 11** SST-SAS simulation of the turbulent flow around the NACA0021 airfoil [48]. Mean surface pressure coefficient.  $\alpha = 60^\circ$ ,  $Re = 2.7 \times 10^5$ . Grid of  $140 \times 101 \times 134 \approx 1.9 \times 10^6$  points. (Courtesy of Egorov et al. [48])



denoted EXPANS. In both approaches, relatively to the RANS equations (13) and (14), the corresponding subfilter-scale equations (122) and (124) look like identical to the RANS equations but the coefficient  $c_{\epsilon_{sfs2}}$  appearing in the destruction term of the dissipation-rate is no longer constant whereas the coefficient  $c_{\epsilon_{sfs1}}$  is the same as the RANS coefficient  $c_{\epsilon_1}$ . In PITM, the coefficient  $c_{\epsilon_{sfs2}}$  is given by Eq. 118 whereas in PANS, it is obtained from Eq. 138 which recovers the original PITM formulation considering that  $f_\epsilon$  reduces to unity. In practice, the PITM method was used to derive both two-equation subfilter scale models [26, 29] as well as seven equation subfilter scale stress models [27, 30–36] and is amenable to the derivation of companion subfilter models for almost any usual RANS model. Up to now, the PANS method was mainly applied to devise two-equation subfilter models [39, 40] as well as four equation subfilter models [43]. These methods were used to simulate both internal and external flows encountered in engineering applications. The new EXPANS method of Foroutan and Yavuzkurt was applied with success to swirling confined flows [45].

### 8.2 DES and PITM methods

The DES method has been shortly described previously. It is usually based on a single transport equation for effective turbulence viscosity or on a  $k - \epsilon$  type model and has provided very convenient and successful practical applications in the engineering area. Friess et al. [134] have shown that in the case of two equation models, an empirical modification of the dissipation rate  $\epsilon$  can lead to an equivalent formulation to PITM, provided some assumptions are made, as demonstrated in detail in Ref. [134]. Obviously, the equivalence property is concerned with the ensemble-averaged filtered equations (110) and (112) and not with the filtered instantaneous equations (122) and (124). The authors Friess et al. [134] have introduced the general concept of H-equivalence where  $H$  stands for *hybrid* that allows to view different hybrid methods as a model of the same system of equations. The comparison between DES and PITM is then based on this H-equivalence property [134] which relies on the postulate that two hybrid methods based on the same closure, but using a different method of control of the energy partition yield similar low-order statistics of the resolved velocity fields provided that they yield the same level of subfilter energy. According to these authors [134], this postulate must be admitted to establish the H-equivalence between DES and PITM by means of analytical developments. For both methods, the ensemble-averaged filtered transport equations for the subfilter energy and dissipation-rate can be formally rewritten in the compact form as

$$\frac{\partial \langle k_{sfs} \rangle}{\partial t} = \langle P_{sfs} \rangle - \psi \langle \epsilon_{sfs} \rangle + \langle J_{sfs} \rangle \tag{145}$$

and

$$\frac{\partial \langle \epsilon_{sfs} \rangle}{\partial t} = c_{\epsilon_1} \frac{\langle \epsilon_{sfs} \rangle}{\langle k_{sfs} \rangle} \langle P_{sfs} \rangle - c_{\epsilon_2}^* \frac{\langle \epsilon_{sfs} \rangle^2}{\langle k_{sfs} \rangle} + \langle (J_\epsilon)_{sfs} \rangle \tag{146}$$

For PITM,  $\psi = 1$  and  $c_{\epsilon_2}^* = c_{sfs\epsilon_2}$  is given by Eq. 118 whereas for DES,  $\psi = F_{DES}$  as defined in Eq. 102 and  $c_{\epsilon_2}^* = c_{\epsilon_2}$ . The theoretical analysis has been conducted in different cases of turbulent flows and different expressions of the function  $\psi$  were devised to get the equivalence criterion between DES and PITM. As a result, Friess et al. [134] have demonstrated that the DES method is H-equivalent to the PITM method if the length-scale  $L_{H-DES}$  is computed as

$$L_{H-DES} = \frac{1}{\psi} \left( \frac{\langle k_{sfs} \rangle}{k} \right)^{3/2} \frac{k^{3/2}}{\epsilon} \tag{147}$$

where  $\psi$  is given by

$$\psi = 1 + \frac{1}{c_{\epsilon_1}}(c_{\epsilon_2} - c_{\epsilon_1}) \left[ 1 - \left( \frac{\langle k_{sfs} \rangle}{k} \right)^{c_{\epsilon_1}/c_{\epsilon_2}} \right] \quad (148)$$

provided however that the dissipation-rate is independent on the cutoff wave number  $\kappa_c$ . If the cutoff wave number occurs in the inertial zone of the spectrum, it is simply matter then to see by using Eq. 131 that the equivalent coefficient  $C_{H-DES}$  must be given by

$$C_{H-DES} = \frac{1}{\beta_0^{3/2} \pi \psi} \quad (149)$$

which is now dependent of the ratio  $\langle k_{sfs} \rangle / k$  instead of being the constant numerical coefficient  $C_{DES}$  used in standard DES,  $\beta_0 = 2/(3C_K)$ . The length-scale in standard DES is a simple linear approximation of Eq. 149, called equivalent-DES. To illustrate their results, these authors have performed the fully turbulent channel flow at the friction Reynolds number  $R_\tau = 395$  as well as the well known test case of the flow over periodic hills at the Reynolds number  $Re = 10595$  using both the PITM method and the equivalent-DES method where  $F_{DES}$  is here given by

$$F_{DES} = \max \left( 1, \frac{k_{sgs}^{3/2} / \epsilon_{sgs}}{L_{H-DES}} \right) \quad (150)$$

These methods were implemented in a framework of a second moment closure accounting for transport equations of the subfilter-scale stresses  $(\tau_{ij})_{sfs}$ . As a result, both simulations returned mean velocity and stress profiles that are close from each other, with a similar partition of turbulent energy as shown in Figs. 6–8 of Ref. [134]. These authors then suggested that the equivalence criteria can be valid beyond the restrictive framework of equilibrium flows [134].

## 9 Concluding Remarks

In this paper, we have analyzed the RANS and LES methodologies and we have then proposed a theoretical formalism developed in the spectral space that allows to unify these two apparently different approaches. Then, considering these various hybrid RANS/LES methods that have been developed often independently from each other using theoretical or empirical arguments, we have investigated the main hybrid methods that are currently used for the simulation of turbulent flows. In particular, we have focused attention on the very large eddy simulation, the detached eddy simulation, the partially integrated transport modeling method, the partially averaged Navier-Stokes method and the scale adaptive simulation. The performances and drawback of these methods were mentioned with some illustrations of turbulent flows encountered in engineering applications. Although these hybrid methods appear different at a first sight, we have shown that it is still possible to establish a link between several schools, PITM and EXPANS as well as DES and PITM, provided some assumptions are made. Overall, the author felt that the choice of applying a given model rather than another one is not only governed by the intrinsic performances of the model itself but it depends also of the type of the physical phenomena acting in the turbulent flow and the answers that are expected to the problem. In that sense, it is clear that the most appropriate method for one particular application will depend on the expectations of the engineer and the computational resources the applicant is prepared to expend

on the problem. The computational framework, academic or industrial, is of course very influential. That being said, the author tends to favor hybrid non-zonal RANS/LES models evolving continuously from the RANS to LES mode with the same formulation of equations depending both on the grid-size  $\Delta$  and the flow characteristics, instead of zonal models for which the basic formulation changes across the artificial interface separating the RANS and LES regions where the so called gray zone still poses some overwhelming problems. Models based on theoretical arguments appear more satisfactory than models built on empirical or practical arguments, at least in principle, even if an empirical model might return better results than a more rational model for one specific test case. The ideal choice would be to get the larger degree of universality in a model based on a consistent formalism that works relatively well against a large variety of turbulent flows. An important point that must be pointed out about hybrid methods is the grid resolution. Considerably coarsening the mesh for reducing the computational time and memory resource has the effect to move the cutoff wavenumber  $\kappa_c$  of the simulation earlier in the inertial zone of the energy spectrum. In that case, an higher part of subgrid-scale energy must be modeled in comparison with the one associated with conventional LES. Then, the turbulent scales that are smaller than the grid size  $\Delta$  cannot anymore be considered as locally isotropic because intermediate scales between the large scales and small scales are included in this part of energy. In this situation, it seems judicious to apply advanced closure models capable of reproducing a realistic description of the subgrid flow anisotropy. Hybrid RANS/LES methods are a very active field of research. This paper tries to bring to light some leading features of the hybrid methods studied here with both theoretical and practical elements aiming to guide the user involved in CFD in his choice of the appropriate turbulence model.

**Acknowledgements** I am grateful to Dr. Roland Schiestel for his comments on this manuscript and his partnership over the many years.

### Compliance with Ethical Standards

**Conflict of interests** The author declares that he has no conflict of interest.

## References

1. Geurts, B.J.: Elements of direct and large-eddy simulation. Edwards (2004)
2. Lesieur, M., Métais, O., Comte, P.: Large-eddy Simulations of Turbulence. Cambridge University Press (2005)
3. Pope, S.B.: Turbulent Flows. Cambridge University Press, Cambridge (2000)
4. Leschziner, M., Li, M.N., Tessicini, F.: Simulating flow separation from continuous surfaces: Routes to overcoming the Reynolds number barrier. *Phil. Trans. R. Soc. A* **367**, 2885–2903 (2009)
5. Choi, H., Moin, P.: Grid-point requirements for large eddy simulation: Chapman’s estimates revisited. *Phys. Fluids* **24**, 011702, 1–5 (2012)
6. Pope, S.B.: Ten questions concerning the large-eddy-simulation of turbulent flows. *New J. Phys.* **6**, 35, 1–24 (2004)
7. Gatski, T.B., Rumsey, C.L., Manceau, R.: Current trends in modelling research for turbulent aerodynamic flows. *Philos. Trans. R. Soc. London, Ser. A* **365**, 2389–2418 (2007)
8. Schiestel, R.: Modeling and Simulation of Turbulent Flows. ISTE Ltd and J Wiley (2008)
9. Hanjalic, K., Launder, B.E.: Modelling Turbulence in Engineering and the Environment. Second-moment Route to Closure. Cambridge University Press (2011)
10. Hanjalic, K., Jakirlic, S.: Contribution towards the second-moment closure modeling of separating turbulent flows. *Comput. Fluids* **27**, 137–156 (1998)
11. Leschziner, M.A., Drikakis, D.: Turbulence modelling and turbulent-flow computation in aeronautics. *Aeronaut. J.* **106**, 349–383 (2002)

12. Chaouat, B.: Reynolds stress transport modeling for high-lift airfoil flows. *AIAA J.* **44**, 2390–2403 (2006)
13. Sagaut, P., Deck, S., Teracolli, M.: *Multiscale and Multiresolution Approaches in Turbulence*, 2nd edn. Imperial College Press, London (2013)
14. Fröhlich, J., Von Terzi, D.: Hybrid LES/RANS methods for the simulation of turbulent flows. *Prog. Aerosp. Sci.* **44**, 349–377 (2008)
15. Speziale, C.G.: Turbulence modeling for time-dependent RANS and VLES: A review. *AIAA J.* **36**, 173–184 (1998)
16. Fasel, H.F., Seidel, J., Wernz, S.: A methodology for simulations of complex turbulent flows. *J. Fluids Eng. ASME* **124**, 933–942 (2002)
17. Spalart, P.R., Jou, W., Strelets, M., Allmaras, S.R.: Comments on the feasibility of LES for wings, and on a hybrid RANS/LES approach. In: Liu, C., Liu, Z. (eds.) *Advances in DNS/LES*, pp. 137–147. Greyden Press, Columbus (1997)
18. Travin, A., Shur, M.L., Strelets, M., Spalart, P.: Detached-eddy simulations past a circular cylinder. *Flow Turbul. Combust.* **63**, 293–313 (1999)
19. Spalart, P.R.: Strategies for turbulence modelling and simulations. *Int. J. Heat Fluid Flow* **21**, 252–263 (2000)
20. Spalart, P.R.: Detached-eddy simulation. *Annu. Rev. Fluid Mech.* **41**, 181–202 (2009)
21. Spalart, P.R., Deck, S., Shur, M.L., Squires, K.D., Strelets, M.K., Travin, A.: A new version of detached-eddy simulation, resistant to ambiguous grid densities. *Theor. Comput. Fluid Dyn.* **20**, 181–195 (2006)
22. Shur, M.L., Spalart, P., Strelets, M.K., Travin, A.K.: A hybrid RANS-LES approach with delayed-DES and wall-modelled LES capabilities. *Int. J. Heat Fluid Flow* **29**, 1638–1649 (2008)
23. Strelets, M.: Detached eddy simulation of massively separated flows. *AIAA paper n° 0879*, 1–18 (2001)
24. Travin, A., Shur, M.L.: Physical and numerical upgrades in the detached-eddy simulation of complex turbulent flows. In: Friedrich, R., Rodi, W. (eds.) *Advances in LES of Complex Flows*, pp. 239–254. Kluwer Academic Publishers (2002)
25. Menter, F.R., Kuntz, M., Langtry, R.: Ten years of industrial experience with SST turbulence model. *Turb. Heat Mass Transf.* **4**, 625–632 (2003)
26. Schiestel, R., Dejoan, A.: Towards a new partially integrated transport model for coarse grid and unsteady turbulent flow simulations. *Theor. Comput. Fluid Dyn.* **18**, 443–468 (2005)
27. Chaouat, B., Schiestel, R.: A new partially integrated transport model for subgrid-scale stresses and dissipation rate for turbulent developing flows. *Phys. Fluids* **17**(065106), 1–19 (2005)
28. Chaouat, B., Schiestel, R.: From single-scale turbulence models to multiple-scale and subgrid-scale models by Fourier transform. *Theor. Comput. Fluid Dyn.* **21**, 201–229 (2007)
29. Befeno, I., Schiestel, R.: Non-equilibrium mixing of turbulence scales using a continuous hybrid RANS/LES approach: Application to the shearless mixing layer. *Flow Turb. Combust.* **78**, 129–151 (2007)
30. Chaouat, B., Schiestel, R.: Progress in subgrid-scale transport modelling for continuous hybrid non-zonal RANS/LES simulations. *Int. J. Heat Fluid Flow* **30**, 602–616 (2009)
31. Chaouat, B.: Simulation of turbulent rotating flows using a subfilter scale stress model derived from the partially integrated transport modeling method. *Phys. Fluids* **24**(045108), 1–35 (2012)
32. Chaouat, B., Schiestel, R.: Analytical insights into the partially integrated transport modeling method for hybrid Reynolds averaged Navier-Stokes equations-large eddy simulations of turbulent flows. *Phys. Fluids* **24**(085106), 1–34 (2012)
33. Chaouat, B., Schiestel, R.: Partially integrated transport modeling method for turbulence simulation with variable filters. *Phys. Fluids* **25**(125102), 1–39 (2013)
34. Chaouat, B.: Subfilter-scale transport model for hybrid RANS/LES simulations applied to a complex bounded flow. *J. Turbul.* **11**, 1–30 (2010)
35. Chaouat, B., Schiestel, R.: Hybrid RANS-LES simulations of the turbulent flow over periodic hills at high Reynolds number using the PITM method. *Comput. Fluids* **84**, 279–300 (2013)
36. Chaouat, B.: Application of the PITM method using inlet synthetic turbulence generation for the simulation of the turbulent flow in a small axisymmetric contraction. *Flow Turbul. Combust.* **98**, 987–1024 (2017)
37. Girimaji, S.S., Srinivasan, R., Jeong, E.: PANS turbulence for seamless transition between RANS and LES: Fixed-point analysis and preliminary results. *Proc. ASME FEDSM'03*, ASME paper n° **45336**, 1–9 (2003)
38. Girimaji, S.S., Abdol-Hamid, K.: Partially averaged Navier Stokes model for turbulence: Implementation and validation. *AIAA paper n° 0502*, 1–14 (2005)
39. Girimaji, S.S.: Partially-averaged Navier-Stokes method for turbulence: A Reynolds-averaged Navier-Stokes to direct numerical simulation bridging method. *J. Appl. Mech., ASME* **73**, 413–421 (2006)

40. Girimaji, Jeong, E., Srinivasan, R.: Partially averaged Navier-Stokes method for turbulence: Fixed point analysis and comparisons with unsteady partially averaged Navier-Stokes. *J. Appl. Mech.*, ASME **73**, 422–429 (2006)
41. Lakshminpathy, S., Girimaji, S.S.: Extension of Boussinesq turbulence constitutive relation for bridging methods. *J. Turbul.* **8**(31), 1–20 (2007)
42. Jeong, E., Girimaji, S.S.: Partially averaged Navier-Stokes (PANS) method for turbulence simulations-Flow past a square cylinder. *J. Fluids Eng.*, ASME **132**(1212203), 1–11 (2010)
43. Basara, B., Krajnovic, S., Girimaji, S., Pavlovic, Z.: Near-wall formulation of the partially averaged Navier-Stokes turbulence model. *AIAA J.* **42**(12), 2627–2636 (2011)
44. Krajnovic, S., Lárusson, R., Basara, B.: Superiority of PANS compared to LES in predicting a rudimentary landing gear flow with affordable meshes. *Int. J. Heat Fluid Flow* **37**, 109–122 (2012)
45. Foroutan, H., Yavuzkurt, S.: A partially averaged Navier Stokes model for the simulation of turbulent swirling flow with vortex breakdown. *Int. J. Heat Fluid Flow* **50**, 402–416 (2014)
46. Menter, F.R., Egorov, Y.: A scale-adaptive simulation model using two-equation models. *AIAA paper n° 1095*, 1–13 (2005)
47. Menter, F.R., Egorov, Y.: The scale-adaptive simulation method for unsteady turbulent flow prediction: Part 1: Theory and model description. *Flow Turbul. Combust.* **85**, 113–138 (2010)
48. Egorov, Y., Menter, F.R., Lechner, R., Cokljat, D.: The scale-adaptive simulation method for unsteady turbulent flow prediction: Part 2: Application to complex flows. *Flow Turbul. Combust.* **85**, 139–165 (2010)
49. Hanjalic, K., Hadžiabdic, M., Temmerman, L., Leschziner, M.: Merging LES and RANS strategies: Zonal or seamless coupling? In: Friedrich, R., Geurts, B., Méttais, O. (eds.) *Direct and Large Eddy Simulation*, V, pp. 451–464. Kluwer Academic Publishers (2004)
50. Hanjalic, K.: Will RANS survive LES? A view of perspectives. *J. Fluids Eng.*, ASME **127**, 831–839 (2005)
51. Hanjalic, K., Kenjeres, S.S.: Some developments in turbulence modeling for wind and environmental engineering. *J. Wind Eng Indus Aerodyn* **96**, 1537–1570 (2008)
52. Kim, J., Moin, P., Moser, R.: Turbulence statistics in fully developed channel flow at low Reynolds number. *J. Fluid Mech.* **177**, 133–166 (1987)
53. Moser, R., Kim, J., Mansour, N.: Direct numerical simulation of turbulent channel up to  $Re_\tau = 590$ . *Phys. Fluids* **11**(4), 943–945 (1999)
54. Hoyas, S., Jimenez, J.: Scalling of velocity fluctuations in turbulent channels up to  $Re_\tau = 2003$ . *Phys. Fluids* **18**(011702), 1–4 (2006)
55. Kaneda, Y., Ishihara, T.: High-resolution direct numerical simulation of turbulence. *J. Turbul.* **7**, 1–17 (2006)
56. Speziale, C.G.: Analytical methods for the development of Reynolds stress closures in turbulence. *Ann. Rev J. Fluid Mech.* **23**, 107–157 (1991)
57. Launder, B.E.: Second moment closure: Present and future. *Int. J. Heat Fluid Flow* **20**(4), 282–300 (1989)
58. Gatski, T.B., Speziale, C.G.: On explicit algebraic stress models for complex turbulent flows. *J. Fluid Mech.* **254**, 59–78 (1993)
59. Spalart, P.R., Allmaras, S.R.: A one-equation turbulence model for aerodynamic flows. *AIAA paper n° 0439*, 1–22 (1992)
60. Spalart, P.R., Allmaras, S.R.: A one-equation turbulence model for aerodynamic flows. *La recherche Aérospatiale* **94**(1), 5–21 (1994)
61. Jones, W.P., Launder, B.E.: The prediction of laminarization with of turbulence. *Int. J. Heat Mass Transfer* **15**, 301–314 (1972)
62. Wilcox, D.C.: Reassessment of the scale-determining equation for advanced turbulence models. *AIAA J.* **26**, 1299–1310 (1988)
63. Menter, F.R.: Two-equation eddy-viscosity turbulence models for engineering application. *AIAA J.* **32**(8), 1598–1605 (1994)
64. Hanjalic, K., Launder, B.E.: A Reynolds stress model of turbulence and its application to thin shear flow. *J. Fluid Mech.* **52**, 609–638 (1972)
65. Launder, B.E., Reece, G.J., Rodi, W.: Progress in the development of a Reynolds stress turbulence closure. *J. Fluid Mech.* **68**, 537–566 (1975)
66. Rotta, J.C.: Statistische theorie nichthomogener turbulenz. *Z. Physik* **129**, 547–572 (1951)
67. Crow, S.C.: Viscoelastic properties of the fine-grained incompressible turbulence. *J. Fluid Mech.* **33**, 1–20 (1968)
68. Speziale, C.G., Sarkar, S., Gatski, T.B.: Modelling the pressure-strain correlation of turbulence: an invariant dynamical approach. *J. Fluid Mech.* **227**, 245–272 (1991)

69. Gatski, T.B.: Second-moment and scalar flux representations in engineering and geophysical flows. *Fluid Dyn. Res.* **41**(012202), 1–24 (2009)
70. Lesieur, M., Metais, O.: New trends in large-eddy simulations of turbulence. *Ann. Rev. J. Fluid Mech.* **28**, 45–82 (1996)
71. Piomelli, U.: Large eddy simulation: Achievement and challenges. *Progress Aeros. Sci.* **35**, 335–362 (1999)
72. Hinze, J.O.: *Turbulence*. Mc Graw-Hill, New York (1975)
73. Smagorinsky, J.: General circulation experiments with the primitive equations. *Mon. Weather Rev.* **91**, 99–165 (1963)
74. Germano, M., Piomelli, U., Moin, P., Cabot, W.H.: A dynamic subgrid-scale eddy viscosity model. *Phys. Fluids A* **3**(7), 1760–1765 (1991)
75. Lilly, D.K.: A proposed modification of the Germano subgrid-scale closure method. *Phys. Fluids A* **3**, 633–635 (1992)
76. Métais, O.M., Lesieur, L.: Spectral large-eddy simulation of isotropic and stably stratified turbulence. *J. Fluid Mech.* **239**, 157–194 (1992)
77. Schumann, U.: Subgrid scale model for finite difference simulations of turbulent flows in plane channels and annuli. *J. Comput. Phys.* **18**, 376–404 (1975)
78. Yoshizawa, A., Horiuti, K.: A statistically derived subgrid scale kinetic model for the large-eddy simulation of turbulent flows. *J. Phys. Soc. Jpn.* **54**(8), 2834–2835 (1985)
79. Horiuti, K.: Large eddy simulation of turbulent channel flow by one-equation modeling. *J. Phys. Soc. Jpn* **54**(8), 2855–2865 (1985)
80. Deardorff, J.W.: The use of subgrid transport equations in a three-dimensional model of atmospheric turbulence. *J. Fluids Eng., ASME* **95**, 429–438 (1973)
81. Deardorff, J.W.: Three-dimensional numerical study of the height and mean structure of heated planetary boundary layer. *Bound.-Layer Meteorol.* **7**, 81–106 (1974)
82. Piomelli, U., Balaras, E.: Wall-layer models for large-eddy simulations. *Annu. Rev. Fluid Mech.* **34**, 349–374 (2002)
83. Piomelli, U., Balaras, E., Pasinato, H., Squires, K.D., Spalart, P.: The inner-outer-layer interface in large-eddy simulations with wall-layer models. *Int. J. Heat Fluid Flow* **24**, 538–550 (2003)
84. Piomelli, U.: Wall-layer models for large-eddy simulations. *Prog. Aerosp. Sci.* **44**, 437–446 (2008)
85. Temmerman, L., Leschziner, M., Mellen, C.P., Fröhlich, J.: Investigation of a wall-function approximations and subgrid-scale models in large eddy simulation of separated flow in a channel with streamwise periodic constrictions. *Int. J. Heat Fluid Flow* **24**, 157–180 (2003)
86. Balaras, E., Benocci, C., Piomelli, U.: Two-layer approximate boundary conditions for large-eddy simulations. *AIAA J.* **34**, 1111–1119 (1996)
87. Schiestel, R.: Sur le concept d'échelles multiples en modélisation des écoulements turbulents, Part I. *J. Theor. Appl. Mech.* **2**(3), 417–449 (1983)
88. Schiestel, R.: Sur le concept d'échelles multiples en modélisation des écoulements turbulents, Part II. *J. Theor. Appl. Mech.* **2**(4), 601–628 (1983)
89. Pruet, C.D., Gatski, T.B., Grosch, C.E., Thacker, W.D.: The temporally filtered Navier-Stokes equations: Properties of the residual stress. *Phys. Fluids* **15**, 2127–2140 (2003)
90. Iovieno, M., Tordella, D.: Variable scale filtered Navier-Stokes equations: a new procedure to deal with the associated commutation error. *Phys. Fluids* **15**, 1926–1936 (2003)
91. Lilly, D.K.: The representation of small scale turbulence in numerical simulation experiments. In: IBM (ed.) *Proceedings of the IBM Scientific Symposium on Environmental Sciences*, pp. 195–210 (1967)
92. Germano, M.: Turbulence: The filtering approach. *J. Fluid Mech.* **238**, 325–336 (1992)
93. Germano, M.: The simplest decomposition of a turbulent field. *Physica D* **241**, 284–287 (2012)
94. Dejoan, A., Schiestel, R.: LES, of unsteady turbulence via a one-equation subgrid-scale transport model. *Int. J. Heat Fluid Flow* **23**, 398–412 (2002)
95. Donaldson, C.: Calculation of turbulent shear flows for atmospheric and vortex motions. *AIAA J.* **10**(1), 4–12 (1972)
96. Jeandel, D., Brison, J.F., Mathieu, J.: Modeling methods in physical and spectral space. *Phys. Fluids* **21**, 169–182 (1978)
97. Cambon, C., Jeandel, D., Mathieu, J.: Spectral modelling of homogeneous non-isotropic turbulence. *J. Fluid Mech.* **104**, 247–262 (1981)
98. Schiestel, R.: Multiple-time scale modeling of turbulent flows in one point closures. *Phys. Fluids* **30**, 722–731 (1987)
99. Schiestel, R., Elena, L.: Modeling of anisotropic turbulence in rapid rotation. *Aerosp. Sci. Technol.* **7**, 441–451 (1997)

100. Hanjalic, K., Launder, B.E., Schiestel, R.: Multiple-time scale concepts in turbulent transport modelling. In: Springer Verlag (ed) Proceedings of the 2th Symposium on Turbulence Shear Flow, pp. 36–49 (1980)
101. Hamba, F.: An attempt to combine large eddy simulation with the  $k - \epsilon$  model in a channel-flow calculation. *Theor. Comput. Fluid Dyn.* **14**, 323–336 (2001)
102. Hamba, F.: A hybrid RANS/LES simulation of turbulent channel flow. *Theor. Comput. Fluid Dyn.* **03**, 387–403 (2003)
103. Davidson, L., Peng, S.H.: Hybrid LES-RANS modelling: A one-equation SGS model combined with a  $k - \omega$  model for predicting recirculating flows. *Int. J. Numer. Meth. Fluids* **43**, 1003–1018 (2003)
104. Temmerman, L., Hadžiabdic, M., Leschziner, M.A., Hanjalic, K.: A hybrid two-layer URANS-LES approach for large eddy simulation at high Reynolds numbers. *Int. J. Heat Fluid Flow* **26**, 173–190 (2005)
105. Jaffrézic, B., Breuer, M.: Application of an explicit algebraic Reynolds stress model within a hybrid LES-RANS method. *Flow Turbul. Combust.* **81**, 415–448 (2008)
106. Schmidt, S., Breuer, M.: Hybrid LES-URANS methodology for the prediction of non-equilibrium wall-bounded internal and external flows. *Comput. Fluids* **96**, 226–252 (2014)
107. Batten, P., Golberg, U., Chakravarthy, S.: Interfacing statistical turbulence closures with large-eddy simulation. *AIAA J.* **42**, 485–492 (2004)
108. Tessicini, F., Temmerman, L., Leschziner, M.A.: Approximate near-wall treatments based on zonal and hybrid RANS-LES methods for LES at high Reynolds numbers. *Int. J. Heat Fluid Flow* **27**, 789–799 (2006)
109. Hamba, F.: Log-layer mismatch and commutation error in hybrid RANS/LES simulation of channel flow. *Int. J. Heat Fluid Flow* **30**, 20–31 (2009)
110. Davidson, L., Billson, M.: Hybrid LES-RANS using synthesized turbulent fluctuations for forcing in the interface region. *Int. J. Heat Fluid Flow* **27**, 1028–1042 (2006)
111. Shur, M.L., Spalart, P.R., Strelets, M.K., Travin, A.K.: Synthetic turbulence generators for RANS-LES interfaces in zonal simulations of aerodynamic and aeroacoustic problems. *Flow Turbul. Combust.* **93**, 63–92 (2014)
112. Fadai-Ghotbi, A., Friess, C., Manceau, R., Gatski, T.B., Borée, J.: Temporal filtering: A consistent formalism for seamless hybrid RANS-LES modeling in inhomogeneous turbulence. *Int. J. Heat Fluid Flow* **31**, 378–389 (2010)
113. Fadai-Ghotbi, A., Friess, C., Manceau, R., Borée, J.: A seamless hybrid RANS-LES model based on transport equations for the subgrid stresses and ellipting blending. *Phys. Fluids* **22**(055104), 1–19 (2010)
114. Walters, D.K., Bhushan, S., Alam, M.F., Thompson, D.S.: Investigation of a dynamic hybrid RANS/LES modelling methodology for finite-volume CFD simulations. *Flow Turbul. Combust.* **91**, 643–667 (2013)
115. Menter, F.R.: A new paradigm in hybrid RANS-LES modeling. In: Proceedings of the 6th Symposium on Hybrid RANS-LES Methods, pp. 1–17 (2016)
116. Hsieh, K., Lien, F., Yee, E.: Towards a unified turbulence simulation approach for wall-bounded flows. *Flow Turbul. Combust.* **84**, 193–218 (2010)
117. Han, X., Krajnović, S.: An efficient very large eddy simulation model for simulation of turbulent flow. *Int. J. Numer. Meth. Fluids* **71**, 1341–1360 (2013)
118. Han, X., Krajnović, S.: Validation of a novel very large eddy simulation method for simulation of turbulent separated flow. *Int. J. Numer. Meth. Fluids* **73**, 436–461 (2013)
119. Han, X., Krajnović, S.: Very-large eddy simulation based on  $k - \omega$  model. *AIAA J.* **53**, 1103–1108 (2015)
120. Forsythe, J.R., Squires, K.D., Wurtzler, K.E., Spalart, P.R.: Detached-eddy simulation of the F-15E at high alpha. *J. Aircraft* **41**(2), 193–200 (2005)
121. Spalart, P.R., Shur, M., Strelets, M., Travin, A.K.: Initial noise predictions for rudimentary landing gear. *J. Sound Vib.* **320**, 4180–4195 (2011)
122. Garbaruk, A.V., Shur, M., Strelets, M.: DDES and IDDES of tandem cylinders. In: Proceedings of the Benchmark Problems for Airframe Noise Computations BANC (2010)
123. Garbaruk, A., Spalart, P.R., Strelets, M., Shur, M.L.: Flow and noise prediction for tandem cylinder. *Matematiceskoe Modelirovanie* **26**(6), 119–136 (2014)
124. Greschner, B., Grillat, J., Jacob, M.C., Thiele, F.: Measurements and wall modeled LES simulation of trailing edge noise caused by a turbulent boundary layer. *Int. J. Aeroacoustics* **9**, 329–355 (2010)
125. Deck, S.: Zonal-detached-eddy simulation of the flow around a high-lift configuration. *AIAA J.* **43**(11), 2372–2384 (2005)

126. Deck, S.: Recent improvements in the zonal detached eddy simulation ZDES formulation. *Theor. Comput. Fluid Dyn.* **26**, 521–550 (2012)
127. Shur, M.L., Spalart, P.R., Strelets, M.K., Travin, A.K.: An enhanced version of DES with rapid transition from RANS to LES in separated flows. *Flow, Turbul. Combust.* **95**, 709–737 (2015)
128. Nikitin, N.V., Nicoud, F., Wasistho, B., Squires, K.D., Spalart, P.R.: An approach to wall modeling in large-eddy simulations. *Phys. Fluids* **12**, 1629–1632 (2000)
129. Garbaruk, A., Strelets, M., Shur, M., Dyadkin, A., Rybak, S.: Numerical investigation of turbulent wake of the nozzles of a launch escape system and computation of pressure fluctuations on the surface of the crew module at different flight conditions. In: *Book of Abstracts of 6th All-Russian Conference, Computational Experiment in Aeroacoustics*, pp 95–99. Svetlogorsk (2016)
130. Kubacki, S., Dick, E.: Simulation of plane impinging jets with  $k - \omega$  based hybrid RANS/LES models. *Int. J. Heat Fluid Flow* **31**, 862–878 (2010)
131. Gritskevich, M.S., Garbaruk, A.V., Schutze, J., Menter, F.R.: Development of DDES and IDDES formulations for the  $k - \omega$  shear stress transport model. *Flow Turbul. Combust.* **88**, 431–449 (2012)
132. Kenjeres, S., Hanjalic, K.: LES, T-RANS and hybrid simulations of thermal convection at high  $Ra$  numbers. *Int. J. Heat Fluid Flow* **27**, 800–810 (2006)
133. Jakirlic, S., Saric, S., Kadavelil, G., Sirubalo, E., Basara, B., Chaouat, B.: SGS modelling in LES of wall-bounded flow using transport RANS model: From a zonal to a seamless hybrid LES/RANS method. In: *Seoul National University (ed.) Proceedings of the 6th Symposium on Turbulence Shear Flow Phenomena*, vol. 3, pp. 1057–1062 (2009)
134. Friess, C., Manceau, R., Gatski, T.B.: Toward an equivalence criterion for hybrid RANS/LES methods. *Comput. Fluids* **122**, 233–246 (2015)
135. Stoellinger, M., Roy, R., Heinz, S.: Unified RANS-LES method based on second-order closure. In: *The University of Melbourne (ed.) Proceedings of the 9th Symposium on Turbulence Shear Flow Phenomena*, vol. 7B5, pp. 1–6 (2015)
136. Apte, S.A., Yang, V.: A large-eddy simulation study of transition and flow instability in a porous-walled chamber with mass injection. *J. Fluid Mech.* **477**, 215–225 (2003)
137. Avalon, G., Casalis, G., Griffond, J.: Flow instabilities and acoustic resonance of channels with wall injection. *AIAA paper n° 3218*, 1–11 (1998)
138. Lamballais, E., Métais, O., Lesieur, M.: Spectral-dynamic model for large-eddy simulations of turbulent rotating flow. *Theor. Comput. Fluid Dyn.* **12**, 149–179 (1998)
139. Dubief, Y., Delcayre, F.: On coherent-vortex identification in turbulence. *J. Turbul.* **1**, 1–22 (2000)
140. Rapp, C., Manhart, M.: Flow over periodic hills - an experimental study. *Exp. Fluids* **51**, 247–269 (2011)
141. Wengle, H., Schiestel, R., Befeno, I., Meri, A.: Large-eddy simulations of the spatial development of a shearless turbulence mixing layer. In: *Numerical Flow Simulation III*, vol. 82, pp. 271–289. Springer, Berlin (2003)
142. Fröhlich, J., Mellen, C.P., Rodi, W., Temmerman, L., Leschziner, M.A.: Highly resolved large-eddy simulation of separated flow in a channel with streamwise periodic constrictions. *J. Fluid Mech.* **526**, 19–66 (2005)
143. Breuer, M., Peller, N., Rapp, C.h., Manhart, M.: Flow over periodic hills. Numerical and experimental study in a wide range of Reynolds numbers. *Comput. Fluids* **38**, 433–457 (2009)
144. Saric, S., Jakirlic, S., Breuer, M., Jaffrezic, B., Deng, G., Chikhaoui, O., Fröhlich, J., Von Terzi, D., Manhart, M., Peller, N.: Evaluation of detached-eddy-simulations for predicting the flow over periodic hills. In: *Cancès, E., Gerbeau, J.F. (eds.) ESAIM Proceedings of CEMRACS 2005 Comput. Aeroacoust. Comput. Fluid Dynam. Turbul. Flows*, vol. 16, pp. 133–145 (2007)
145. Saric, S., Kniesner, B., Mehdizadeh, A., Jakirlic, S., Hanjalic, K., Tropea, C.: Comparative assessment of hybrid LES/RANS models in turbulent flows separating from smooth surfaces. In: *Adv. in Hybrid RANS-LES Modelling, NNFM 97*, pp. 142–151. Springer, Berlin (2008)
146. Ma, J.M., Peng, S.H., Davidson, L., Wang, F.J.: A low Reynolds number variant of partially-averaged Navier-Stokes model for turbulence. *Int. J. Heat Fluid Flow* **32**, 652–669 (2011)
147. Manhart, M., Rapp, C., Peller, N., Breuer, M., Aybay, O., Denev, J., Falconi, J.: Assessment of eddy resolving techniques for the flow over periodically arranged hills up to  $Re=37,000$ . In: *Quality and Reliability of Large Eddy Simulations II*, vol. 16. Springer Verlag, pp 361–370 (2011)
148. Durbin, P.: Near-wall turbulence closure modelling without damping functions. *Theor. Comput. Fluid Dyn.* **3**, 1–13 (1991)
149. Lashmipathy, S., Girimaji, S.S.: Partially averaged Navier-Stokes (PANS) method for turbulence simulations- Flow past a circular cylinder. *J. Fluids Eng., ASME* **132**(1212202), 1–9 (2010)



150. Han, X., Krajnovic, S., Basara, B.: Study of active flow control for a simplified vehicle model using the PANS, method. *Int. J. Heat Fluid Flow* **42**, 139–150 (2013)
151. Mirzaei, M., Krajnovic, S., Basara, B.: Partially-averaged Navier-Stokes simulations of flows around two different Ahmed bodies. *Comput. Fluids* **117**, 273–286 (2015)
152. Krajnović, S., Minelli, G., Basara, B.: Partially-averaged Navier-Stokes simulations of two bluff body flows. *Appl. Math. Comput.* **272**, 692–706 (2016)
153. Menter, F.R.: Elements and Applications of Scale Resolving Simulation Methods in Industrial CFD, Direct and Large Eddy Simulation IX, ERCOFTAC Series 20, pp. 179–196. Springer International Publishing, Switzerland (2015)